

¹ **GLO-Roots: an imaging platform enabling multidimensional characterization of soil-grown root systems**

³ Rubén Rellán-Álvarez^{1, 9}, Guillaume Lobet², Heike Lindner^{1, 8}, Pierre-Luc Pradier^{1, 8, 10},
⁴ Jose Sebastian^{1, 8}, Muh-Ching Yee¹, Yu Geng^{1, 7}, Charlotte Trontin¹, Therese LaRue³,
⁵ Amanda Schrager-Lavelle⁴, Cara H. Haney⁵, Rita Nieu⁶, Julin Maloof⁴, John P. Vogel⁷,
⁶ José R. Dinneny^{1, 12}

⁷ ¹ Department of Plant Biology, Carnegie Institution for Science, Stanford, CA, USA.

⁸ ² PhytoSystems, University of Liège, Liège, Belgium.

⁹ ³ Department of Biology, Stanford University, Stanford, CA, USA.

¹⁰ ⁴ Department of Plant Biology, UC Davis, Davis, CA, USA.

¹¹ ⁵ Harvard Medical School, Massachusetts General Hospital, Department of Genetics, De-
¹² partment of Molecular Biology Boston, MA, USA

¹³ ⁶ USDA Western Regional Research Center, Albany, CA, USA

¹⁴ ⁷ DOE Joint Genome Institute, Walnut Creek, CA, USA

¹⁵ ⁸ These authors contributed equally

¹⁶ ⁹ Present address: Laboratorio Nacional de Genómica para la Biodiversidad (Langebio),
¹⁷ Unidad de Genómica Avanzada, Centro de Investigación y de Estudios Avanzados del Insti-
¹⁸ tuto Politécnico Nacional (CINVESTAV-IPN), Irapuato, Guanajuato, México

¹⁹ ¹⁰ Present address: Boyce Thompson Institute for Plant Research/USDA, Ithaca, NY, USA.

²⁰ ¹¹ Present address: Energy Biosciences Institute, UC, Berkeley, CA, USA

²¹ ¹² Corresponding author

²² **Author contributions:**

²³ RR-A: Conception, design and development of the growth and imaging system and Arabidop-
²⁴ sis transgenic lines; acquisition, analysis and interpretation of data; drafting and revising

25 the article.

26 GL: Development of the GLO-RIA image analysis plugin, analysis and interpretation of

27 data, drafting and revising the article.

28 HL: Acquisition of data, development of the tomato growth and imaging setup.

29 P-LP: Acquisition of data, analysis and interpretation of data

30 JS: Development of Brachypodium transgenic lines, acquisition and analysis of Brachy-

31 podium, Arabidopsis and tomato data.

32 MCY: Development of Arabidopsis and Brachypodium transgenic lines.

33 YG: Development of Arabidopsis transgenic lines.

34 CT: Acquisition and analysis of the QPCR data

35 TL: Acquisition and analysis of the QPCR data

36 AS-L: Contributed the unpublished dual-color tomato line.

37 CH: Contributed the unpublished *Pseudomonas fluorescens* CH267-lux strain.

38 RN: Contribution to the development of the Brachypodium transgenic line.

39 JM: Contributed the unpublished dual-color tomato line.

40 JPV: Contribution to the development of the Brachypodium transgenic line.

41 JRD: Conception, design and development of the growth and imaging system and Arabidop-

42 sis transgenic lines; acquisition, analysis and interpretation of data; drafting and revising

43 the article.

44 All authors read and approve the final version of the manuscript.

45 **Abstract**

46 Root systems develop different root types that individually sense cues from their local

47 environment and integrate this information with systemic signals. This complex multi-

48 dimensional amalgam of inputs enables continuous adjustment of root growth rates, direc-
49 tion and metabolic activity that define a dynamic physical network. Current methods for
50 analyzing root biology balance physiological relevance with imaging capability. To bridge
51 this divide, we developed an integrated imaging system called Growth and Luminescence
52 Observatory for Roots (GLO-Roots) that uses luminescence-based reporters to enable stud-
53 ies of root architecture and gene expression patterns in soil-grown, light-shielded roots. We
54 have developed image analysis algorithms that allow the spatial integration of soil properties,
55 gene expression and root system architecture traits. We propose GLO-Roots as a system
56 that has great utility in presenting environmental stimuli to roots in ways that evoke natural
57 adaptive responses and in providing tools for studying the multi-dimensional nature of such
58 processes.

59 **Introduction**

60 Plant roots are three-dimensional assemblies of cells that coordinately monitor and acclimate
61 to soil environmental change by altering physiological and developmental processes through
62 cell-type and organ-specific regulatory mechanisms^{1,2}. Soil comprises a complex distribution
63 of particles of different size, composition and physical properties, airspaces, variation in
64 nutrient availability and microbial diversity^{3,4}. These physical, chemical and biological
65 properties of soil can vary on spatial scales of meters to microns, and on temporal scales
66 ranging from seasonal change to seconds. Root tips monitor this environment through
67 locally and systemically acting sensory mechanisms^{5,6}.

68 The architecture of the root system determines the volume of soil where resources can be
69 accessed by the plant (rhizosphere) and is under both environmental and genetic control.
70 Plasticity in growth parameters allows the plant to adjust its form to suit a particular soil.
71 Lateral roots, which usually make up the majority of the total root system, often grow at an
72 angle divergent from the gravity vector. This gravity set-point angle (GSA) is controlled by
73 auxin biosynthesis and signaling and can be regulated by developmental age and root type⁷.
74 Recent cloning of the *DRO1* Quantitative Trait Locus (QTL) demonstrates that natural

75 genetic variation is a powerful tool for uncovering such control mechanisms⁸.

76 Specific root ideotypes (idealized phenotypes) have been proposed to be optimal for acquisition
77 of water and nitrogen, which are distinct from ideotypes for low phosphorus. Based on
78 computational modeling and field studies, the “steep, deep and cheap” ideotype proposed by
79 Lynch and colleagues may provide advantages to the plant for capturing water and elements
80 like nitrogen that are water soluble and therefore tend to move in the soil column with water.
81 This ideotype consists of highly gravitropic, vertically oriented roots that grow deep in the
82 soil column and develop large amounts of aerenchyma, which reduces the overall metabolic
83 cost of the root system³. Other nutrients, like phosphorus, which have limited water solubility and are tightly bound to organic matter, usually accumulate in the top layers of soil
84 and favor root systems that are more highly branched and shallow. The low-phosphorus
85 ideotype effectively increases root exploration at the top layers of soil³. Modeling of root
86 system variables shows that optimum architecture for nitrogen and phosphorus uptake are
87 not the same⁹ and suggests tradeoffs that may affect the evolution of root architecture as a
88 population adapts to a particular environmental niche¹⁰.

89

90 Clearly, understanding the architecture of root systems and how environmental conditions
91 alter root developmental programs is important for understanding adaptive mechanisms of
92 plants and for identifying the molecular-genetic basis for different response programs. In
93 addition, root systems have complexity beyond their architecture that needs to be incorporated
94 into our understanding of plant-environment interactions. Primary and lateral roots
95 exhibit different stress response programs in *Arabidopsis*^{2,11} and may play specialized roles
96 in water and nutrient uptake. Thus, it is important to develop methods that allow for a
97 multidimensional characterization of the root system that includes growth, signaling, and
98 interactions with other organisms. Furthermore, physiological parameters that affect whole
99 plant responses to the environment, such as transpiration, are likely integrated into such
100 processes, thus requiring a more holistic approach to studies of root function.

101 Based on these considerations we have developed a new root imaging platform, Growth
102 and Luminescence Observatory for Roots (GLO-Roots), which allows root architecture and

103 gene expression to be studied in soil-grown plants. GLO-Roots is an integrated system
104 composed of custom growth vessels, luminescent reporters and imaging systems. We use
105 rhizotrons that have soil volumes equivalent to small pots and support growth of Arabidopsis
106 from germination to senescence. To visualize roots, we designed plant-codon optimized
107 luciferase reporters that emit light of different wavelengths. To visualize reporter expression,
108 plants are watered with a dilute luciferin solution and imaged afterwards. We have built
109 a custom luminescence imaging system that automatically captures images of rhizotrons
110 held vertically. The signal from each reporter is distinguished using band-pass filters held
111 in a motorized filter wheel, which enables automated acquisition of images from plants
112 expressing both structural and environmentally and developmentally responsive reporters.
113 We have also developed GLO-RIA (GLO-Roots Image Analysis), an ImageJ¹² plugin that
114 allows for automated determination of (among other traits) root system area, convex hull,
115 depth, width and directionality, which quantifies the angle of root segments with respect
116 to gravity. GLO-RIA is also able to relate root system parameters to local root-associated
117 variables such as reporter expression intensity and soil-moisture content.

118 Overall GLO-Roots has great utility in presenting environmental stimuli to roots in phys-
119 iologically relevant ways and provides tools for characterizing responses to such stimuli at
120 the molecular level in whole adult root systems over broad time scales.

121 **Box 1.**

122 All resources for GLO-Roots, including the original raw data used in the manuscript, sample
123 images, GLO-RIA user manual, the latest software updates and the source code, can be
124 found at: <https://dinnenylab.wordpress.com/glo-roots/>

125 **Results.**

126 We have developed an integrated platform for growing, imaging and analyzing root growth
127 that provides advances in physiological relevance and retains the ability to visualize aspects

¹²⁸ of root biology beyond structure.

¹²⁹ **The GLO-Roots platform.**

¹³⁰ GLO-Roots is comprised of four parts: i) growth vessels called rhizotrons that allow plant
¹³¹ growth in soil and root imaging; ii) luminescent reporters that allow various aspects of root
¹³² biology to be tracked in living plants; iii) GLO1 luminescence-imaging system designed to
¹³³ automatically image rhizotrons; iv) GLO-RIA, an image analysis suite designed to quantify
¹³⁴ root systems imaged using GLO-Roots.

¹³⁵ **Plant growth system.** GLO-Roots utilizes custom designed growth vessels classically
¹³⁶ known as rhizotrons, which hold a thin volume of soil between two sheets of polycarbonate
¹³⁷ plastic. Acrylic spacers provide a 2-mm space in which standard peat-based potting mix
¹³⁸ is added. Black vinyl sheets protect roots from light and rubber U-channels clamp the rhi-
¹³⁹ zotron materials together. Plastic racks hold the rhizotrons vertically and further protect
¹⁴⁰ the roots from light. Rhizotrons and rack are placed in a black tub and water is added, to
¹⁴¹ a depth of about 2 cm, at the bottom to maintain moisture in the rhizotrons during plant
¹⁴² growth. The volume of soil in the rhizotrons (100 cm^3) is similar to small pots commonly
¹⁴³ used for *Arabidopsis* and supports growth throughout the entire life cycle (Fig 1A-C and
¹⁴⁴ Supplement 1).

¹⁴⁵ To determine how the biology of plants grown in rhizotrons compares to other standard
¹⁴⁶ growth systems, we utilized high-throughput qRT-PCR to study how these conditions af-
¹⁴⁷ fect expression of 77 marker genes in root and shoot samples. These genes were curated
¹⁴⁸ from the literature and belong to a wide array of biological pathways including nutrient
¹⁴⁹ acquisition, hormone and light response and abiotic stress. Whole roots and shoot samples
¹⁵⁰ were collected at the end of the light and dark periods (Long-day conditions: 16 hour light,
¹⁵¹ 8 hours dark) from plants grown in rhizotrons, pots, and petri dishes with two different
¹⁵² media compositions: 1X Murashige and Skoog basal salts (ms) 1% sucrose or 0.25X ms,
¹⁵³ no sucrose (ms25). Principal component analysis of the gene expression values showed a
¹⁵⁴ separation of soil and gel-grown root systems in the the first principal components (Figure

155 1-figure supplement 1A). In roots grown on gel-based media, we observed enhanced expres-
156 sion of genes associated with light-regulated pathways (flavonoid biosynthesis: *FLAVINOL*
157 *SYNTHASE1*, *FLS1*, *CHALCONE SYNTHASE*, *CHS* and photosynthesis: *RUBISCO SUB-*
158 *UNIT 1A*, *RBCS1A*, *CYCLOPHILIN 38*, *CYP38*), which is expected due to the exposure
159 of gel-grown roots to light. In addition, genes associated with phosphorus nutrition (*LOW*
160 *PHOSPHATE RESPONSE1*, *LPR1*, *PHOSPHATE STARVATION RESPONSE1*, *PHR1*)
161 were (Figure 1-figure table supplement 1) less expressed in soil-grown roots, suggesting dif-
162 ferences in nutrient availability between the different growth systems. Interestingly, shoot
163 samples where not as clearly separated by growth media and, instead, time of day had a
164 greater effect (Figure 1-Supplement 2). These data suggest root systems may be partic-
165 ularly sensitive to media conditions and indicate that rhizotron-grown root systems more
166 closely approximate the biology of pot-grown plants than standard gel-based media. Shoot
167 weight and primary root length were significantly reduced for gel-grown plants compared
168 to rhizotron- or pot-grown plants suggesting significant differences in the biology of plants
169 grown under these conditions (Figure 1-figure supplement 1B-C).

170 While the 2 mm depth of the soil sheet is 10 to 20 times the average diameter of an Arabidop-
171 sis root (between 100-200 microns¹³), we evaluated whether rhizotron-grown plants exhibited
172 any obvious stress as a consequence of physical constriction. We compared traits of plants
173 growing in vessels that hold similar volumes of soil but in different volumetric shapes. The
174 number of lateral roots was significantly lower in pot and cylinder-grown plants compared
175 to rhizotron-grown plants (Figure 1-figure supplement 1D) whereas primary root length of
176 rhizotron and cylinder-grown plants was significantly greater than pot-grown plants (Figure
177 1-figure supplement 1E). No significant differences in shoot area were observed between the
178 three systems (Figure 1-figure supplement 1-data). Thus, these data do not support the
179 hypothesis that rhizotron-grown plants experience physical constriction greater than other
180 vessels holding the same volume of soil.

181 **Generation of transgenic plants expressing different luciferases.** Arabidopsis roots
182 cannot easily be distinguished from soil using brightfield imaging due to their thinness and

183 translucency (Figure 1-figure supplement 3); thus, reporter genes are needed to enhance the
184 contrast between the root and their environment. Luciferase is an ideal reporter to visualize
185 roots: 1) unlike fluorescent reporters, luciferase does not require high-intensity excitation
186 light, which could influence root growth, 2) peat-based soil (a type of histosol) exhibits no
187 autoluminescence but does autofluoresce at certain excitation wavelengths similar to GFP
188 (Figure 1-figure supplement 3), 3) while GFP is very stable, and thus not as suitable for
189 imaging dynamic transcriptional events, the luciferase enzyme is inactivated after catabolism
190 of luciferin, making it ideal for studying processes such as environmental responses. A
191 considerable number of luciferases have been developed that emit light spanning different
192 regions of the visible spectrum, but their utilization has been limited to studies in animals
193 (Table 1).

194 To determine the efficacy of using luciferase to visualize roots in soil, we codon optimized
195 sequences of *PpyRE8*, *CBGRed*, *LUC2*, and *CBG99* for Arabidopsis expression. In addition,
196 nanoLUC¹⁴ and venus-LUC2¹⁵ were utilized. Constitutive luciferase expression was driven
197 in plants using the *UBIQUITIN 10* (*UBQ10*) or *ACTIN2* (*ACT2*) promoters using vectors
198 assembled through a Golden-Gate cloning system¹⁶. Plants homozygous for a single locus
199 T-DNA insertion were evaluated for in vivo emission spectra and luminescence intensity
200 (Fig 1D). All the evaluated luciferases use D-luciferin as a substrate facilitating the simulta-
201 neous imaging of different luciferases except nanoLUC, which uses a proprietary substrate
202 furimazine¹⁴. Luciferases with red-shifted emission spectra were less intense than the green-
203 shifted luciferases (Fig 1D). LUC2o showed an emission maximum at 580 nm and a minor
204 peak at 620 nm while CBG99o lacks the minor peak.

205 Continuous addition of luciferin did not have any significant effect on shoot weight or primary
206 root length (Figure 1-figure supplement 4). After luciferin addition, luminescence signal
207 could be reliably detected in root systems for up to 10 days, depending on the developmental
208 state of the plant.

GLO1: a semi-automated luminescence imaging system for rhizotrons. Luminescence imaging systems commercially available for biomedical research are usually optimized for imaging horizontally held specimens or samples in microtiter plates. Placing rhizotrons in this position would induce a gravitropic response in plants. Working with Bioimaging Solutions (San Diego, CA) we designed and built a luminescence imaging system optimized for rhizotron-grown plants. GLO1 (Growth and Luminescence Observatory 1) uses two PIXIS-XB back-thinned CCD cameras (Princeton Instruments, Trenton, NJ, USA) to capture partially-overlapping images of rhizotrons while a motorized stage automatically rotates the rhizotron to capture images of both sides (Fig 1E). A composite image is generated from the images captured of each side; Fig 1F shows that approximately half of the root system is revealed on each side with few roots being visible on both sides. Apparently, the soil sheet is thick enough to block portions of the root system but thin enough to ensure its continuous structure can be compiled from opposite face views. We tested the ability of GLO1-generated images to reveal complete root systems by manually quantifying the number of lateral roots in excavated root systems of 8 different plants and testing these results against estimates of lateral root number from images of the same plants visually inspected by 4 different persons. These comparisons revealed good correlation ($(R^2 = 0.974)$) between actual lateral root counts and image-based estimation, indicating GLO1-generated root images provide an accurate representation of the in soil root system.

GLO-RIA: GLO-Roots Image Analysis. We developed a set of image analysis algorithms that were well suited for the complex root systems that GLO-Roots is able to capture. GLO-RIA (Growth and Luminescence Observatory Root Image Analysis) is an ImageJ plugin divided in two modules. The first module (RootSystem) performs four different types of analysis: i) a local analysis that detects all root particles in the image and computes their position, length and direction; ii) the global analysis performs a root system level analysis and computes the total visible surface, convex hull, width and depth; iii) the shape analysis uses Elliptic Fourier Descriptors or pseudo-landmarks similarly to RootScape¹⁷ to perform a shape analysis on the root

237 system iv) the directionality analysis computes the mean direction of root particles in a
238 root system (either on the full image or by a user-defined region of interest in the image).

239 These four analysis methods are fully automated by default, but can be manually adjusted
240 if needed.

241 The second module of GLO-RIA (RootReporter) was specifically designed for the analysis of
242 multi-layered images such as combinations of gene reporter, root structure and soil moisture.

243 Shortly, the plugin works as follows: i) detection of the gene reporters and the structure
244 reporters in their respective images; ii) if needed, a manual correction can be performed to
245 correct the automated detection; iii) gene reporters are linked with the soil water content
246 and the structure reporters, based on their proximity; iv) gene reporter intensity (either
247 absolute or normalized using the structural reporter) is computed; v) all data are exported

248 and saved to a Root System Markup Language (RSML) datafile¹⁸. Gene and structure
249 reporters can be followed across different time and space points. Using an object oriented

250 approach, great care has been taken to facilitate the user interactions on the different images
251 to streamline the analysis process. Table 2 shows a list of root system features extracted

252 using GLO-RIA. GLO-RIA does not currently have the ability to reconstruct the root archi-
253 tecture in itself (topological links between roots). This is a challenge for analyzing images
254 captured by GLO-Roots since soil particles cause disruption of root segments.

255 We tested the accuracy of the measurements obtained from GLO-RIA using two different
256 ground-truthed data sets. Manual measurement of root system width, depth and average

257 lateral root angle was determined by hand using imageJ from an independent set of images
258 corresponding to roots of several Arabidopsis accessions growing in control conditions. We

259 also used ArchiSimple¹⁹ to generate 1240 images of root system models with contrasting sizes
260 and lateral root angles. Since these images are computationally generated, exact determi-

261 nation of root system parameters was possible. For both ground truth data sets, GLO-RIA
262 quantification provided measurements that were well correlated for all all three measured
263 parameters (Figure 1-figure supplement 5D-F). Sample images of real and ArchiSimple gen-
264 erated root images are shown with GLO-RIA-defined directionality color-coding (Figure
265 1-figure supplement 5G-I).

266 Continuous imaging of root growth.

267 The size of our rhizotrons enables undisturbed root system development (before roots reach
268 the sides or the bottom of the rhizotron) for about 21-23 days for the Col-0 accession
269 growing under long day conditions (Figure 2); however root traits such as directionality
270 can be observed through later stages of plant development. See 35 DAS root system and
271 directionality in Figure 2A-B. An example of a time series spanning 11 to 21 days after
272 sowing (DAS) of Col-0 roots expressing *ProUBQ10:LUC2o* is shown in Fig 2A and [Video 1](#)
273 with a color-coded time projection shown in Fig 2C. Directionality analysis (Fig 2B) shows
274 a progressive change in root system angles from 0° (vertical) to 45° as lateral roots take
275 over as the predominant root type. Figure 2D shows the evolution over time of several root
276 traits that can be automatically captured by GLO-RIA (depth, width, area) and others that
277 were manually quantified (primary root growth rate or number of lateral roots per primary
278 root).

279 Root system architecture of different *Arabidopsis* accessions.

280 As a proof of concept to estimate the utility of our root imaging system to phenotype
281 adult root system traits, we transformed a small set of accessions (Bay-0, Col-0 and Sha)
282 with the *ProUBQ10:LUC2o* reporter and quantified RSA at 22 DAS (Fig 3A-C). GLO-RIA
283 analysis of these root systems identified several root traits that distinguish Col-0, Bay-0
284 and Sha. Directionality analysis revealed an abundance of steep-angle regions in the root
285 system of Bay while Sha showed an abundance of shallow-angled regions and Col-0 was
286 intermediate (Fig 3D). Bay-0 shows the deepest and narrowest root system leading to the
287 highest depth/width ratio while Sha has the widest root system (Fig 3E). Other root traits
288 such as root system area and the vertical center of mass also showed significant differences
289 (Figure 3-figure supplement 1B). Broad sense heritability values for depth (96.3), area (92.0),
290 depth/width (97.8), width (95.7) and vertical center of mass (95.0) were all higher than 90%.
291 To capture the richness of root architecture shape, we used GLO-RIA to extract pseudo-
292 landmarks describing the shape of the root system (see Materials and Methods for more

293 details) and performed PCA analysis. The first principal component captures differences
294 in the distribution of widths along the vertical axis and separates Col-0 and Sha from Bay-
295 0 root systems. (Fig 3F). Bay-0 shows an homogenous distribution of widths along the
296 vertical axis while Sha and Col-0 are much wider at the top than bottom. PC2 seems to be
297 capturing a relationship between width at the top and total depth and separates Sha root
298 systems which are wide at the top and deep from Col-0 root systems which are wide but
299 not as deep as Sha. Shape information extracted from pseudo-landmarks can distinguish
300 the three different accession using PCA analysis (Fig 3G).

301 **Spectrally distinct luciferases enable gene expression patterns, characterization**
302 **of root system interactions and microbial colonization.**

303 We tested whether spectrally distinct luciferase reporters would enable additional informa-
304 tion besides root architecture to be captured from root systems. Luciferase reporters have
305 been commonly used to study gene expression and these resources can potentially be utilized
306 to study such regulatory events in soil-grown roots. We transformed *ProACT2:PpyRE8o*
307 into two well studied LUC reporter lines: the auxin response reporter line *ProDR5:LUC*²⁰
308 (Figure A-B) and the Reactive Oxygen Species (ROS) response reporter *ProZAT12:LUC*²¹
309 (Figure 4C-D). We implemented in GLO-RIA an algorithm that semi-automatically iden-
310 tifies gene reporter signal and associates this object to the corresponding root structure
311 segment. A graphical representation of the results obtained with Root Reporter can be
312 observed in Figure 4-figure supplement 1. Reporter intensity values along the first 5 mm of
313 root tips can also be observed in Figure 4-figure supplement 2.

314 We then took advantage of our ability to constitutively express two spectrally different lu-
315 ciferases and imaged the overlapping root systems (one expressing *ProUBQ10:LUC2o* and
316 the other *ProACT2:PPy RE8o*). While two root systems were distinguishable using this
317 system (Figure 4-figure supplement 3); measurements of root system area did not reveal a
318 significant effect on root growth when two plants were grown in the same rhizotron, com-
319 pared to one; however, further studies are warranted (Figure 4-figure supplement 3).

320 The GLO-Roots system uses non-sterile growth conditions, which allows complex biotic
321 interactions that may affect responses to the environment. Bacteria themselves can be en-
322 gineered to express luminescent reporters through integration of the LUX operon, which
323 results in luminescence in the blue region of the spectrum and is thus compatible with
324 the plant-expressed luciferase isoforms we have tested. *Pseudomonas fluorescens* CH267²²,
325 a natural *Arabidopsis* root commensal, was transformed with the bacterial LUX operon
326 and used to inoculate plants. Thirteen days after inoculation, we were able to observe
327 bacterial luminescence colocalizing with plant roots. *P. fluorescens* did not show an ob-
328 vious pattern of colonization at the root system scale level. As a proof-of-principle test
329 of the multi-dimensional capabilities of the GLO-Roots system we visualized both *LUC2o*
330 and *PPyRE8o* reporters in plants and the LUX reporter in bacteria in the same rhizotron
331 (Figure 4-figure supplement 4).

332 **Adaptive changes in root system architecture under water deprivation, phospho-**
333 **rus deficiency and light.** To test the utility of the GLO-Roots system to understand
334 response of root systems to environmental stimuli we tested the effects of light and condi-
335 tions that mimic drought and nutritional deficiency. To examine the effects of light exposure
336 on the root architecture, the black shields, which normally protect the soil and roots from
337 light, were removed from the top half of the rhizotrons 10 DAS. Using directionality analysis
338 we detected a significant increase in the steepness of roots only in the light exposed region of
339 the rhizotron, while the lower shielded region showed no difference. (Fig 6-figure supplement
340 3A-B and Fig 6-figure supplement 4). Light can penetrate the top layers of soil²³ and it
341 has been proposed to have a role in directing root growth specially in dry soils²⁴ through
342 the blue light receptor *phot1*. Root directionality was not significantly different between
343 light and dark-treated roots of the *phot1/2* double mutant suggesting that blue light per-
344 ception is necessary for this response^{24,25} (Fig 6-figure supplement 3B-lower panel). These
345 data highlight the strong effects of light on root system architecture²⁶, which GLO-Roots
346 rhizotrons are able to mitigate.

347 Plants grown in low-P soil showed a significant increase in the width-depth ratio of the root

348 system compared to plants grown in P-replete soil, as determined using the automated root
349 system area finder in GLO-RIA (Fig 6-figure supplement 2A-B). Plants under P deficiency
350 showed an increase in the ratio between root-shoot area (Fig 6-figure supplement 2C) and
351 higher investment of resources in the development of the root system at the expense of shoot
352 growth (Fig 6-figure supplement 2D). Root systems of control and P-deficient plants showed
353 no significant differences in directionality at 22 DAS but at 27 DAS, roots were more hori-
354 zontally oriented in P-deficient plants (Fig 6-figure supplement 2E). The observed changes in
355 root architecture are consistent with root system ideotypes that improve phosphorus uptake
356 efficiency.

357 GLO-Roots is especially well suited for studying water-deficit (WD) responses. First, shoots
358 are exposed to the atmosphere and vapor pressure deficit is maintained at levels that allow
359 for transpiration of water from the shoot. Second, soil in rhizotrons is exposed to air at
360 the top and dries from the top-down; drying soil increases the volume occupied by air and
361 reduces contact of root with liquid water, all of which are similar to changes in soil expected
362 in the field during WD. Finally, as peat-based soil dries, its optical properties change, al-
363 lowing moisture content to be approximated from bright-field images. We took advantage
364 of the change in gray-scale pixel intensity to construct a calibration curve (Figure 5-figure
365 supplement 1) that quantitatively relates gray-scale pixel intensity to moisture content (Fig
366 5A); water content can be color coded in images with appropriate look up tables (Fig 5B).
367 Soil color was not affected by the presence or absence of roots (Figure 5-figure supplement
368 2). Using this approach, water content in a rhizotron can be mapped and visualized in 2D
369 (Fig 5C-D). In the example shown, we can observe that a 22 DAS Bay-0 plant depleted
370 soil-moisture content locally around the root system (Figure 5E).

371 We performed several trials to simulate WD in our growth system. Plants were germinated,
372 grown under control conditions then transferred to 29°C and standing water removed from
373 the container holding the rhizotrons starting at 9 DAS or 13 DAS. Elevated temperature
374 combined with water deficit is a common stress that modern crops varieties are poorly
375 adapted to, thus highlighting the importance of examining this combined treatment^{27,28}.

376 Plants were maintained in this WD regime until 22 DAS when luciferin solution was added
377 and the plants imaged. At 13 DAS, lateral roots near the soil surface are already emerged
378 ([Video 1](#), Figure 2A) and 9 days of subsequent WD treatment caused lateral roots to show an
379 increase in gravitropism leading to the development of a root system that were deeper and
380 more vertically oriented (Fig 6A). Roots of Bay-0 plants showed similar responses, though
381 the extent of change was less pronounced since Bay-0 roots are normally more vertically
382 oriented (Fig 6B). Plants transferred at 9 DAS and grown for 13 days under WD showed
383 less lateral root development in the top layer of soil (Fig 6E). At this time point, lateral roots
384 start to emerge ([Video 1](#)) and early drought may lead to growth quiescence or senescence.
385 Careful examination of roots in these regions showed evidence of small lateral root primordia
386 populating the primary root (Figure 6F). After 24 h of re-watering (Figure 6G) these lateral
387 root primordia reinitiated growth (Figure 6H).

388 Time-lapse imaging of the water deficit response showed that changes in root growth direc-
389 tion occurred ahead of the dry soil front [Video 2](#). Using GLO-RIA we were able correlate
390 local water moisture contents with the orientation of root segments. With this approach we
391 observed that root segments in dryer areas of rhizotron grew at steeper root angles (Figure
392 7) than roots in WW regions, though lateral root angle in wetter regions was also affected.
393 These data suggest that both local and systemic signaling is likely involved in redirecting
394 lateral roots deeper during the simulated drought treatments tested here.

395 We also grew plants under WD at control temperatures or under WW conditions at elevated
396 temperature to test the effects of these individual stresses on root architecture. We observed
397 that both conditions were sufficient to induce a change in root directionality indicating that
398 the plant uses similar mechanisms to avoid heat and water-deficit associated stresses (Figure
399 6-figure supplement 1). We next asked which regulatory pathways controlled the observed
400 changes in lateral root directionality during simulated drought. Hydrotropism is a known
401 environmental response that directs root growth towards wet regions of soil. MIZ1 is an
402 essential regulator of hydrotropism; however *miz1* mutants had no significant effect on water
403 deficit-induced changes in root directionality, compared to wild type (Fig 6C), indicating

404 that this response was distinct from hydrotropism. Auxin is an important mediator of
405 gravitropism and auxin treatment causes lateral roots to grow more vertically⁷. Consistent
406 with this role for auxin, mutant plants with loss of function in the auxin receptor TIR1, did
407 not show changes in the root system directionality between WW and WD conditions (Fig
408 6D).

409 **GLO-Roots for Brachypodium and Tomato.**

410 To examine the general applicability of the GLO-Roots system for other species, we intro-
411 duced LUC2o-expressing reporters into the model grass *Brachypodium distachyon* and the
412 crop plant *Lycopersicon esculentum* (tomato). Brachypodium is well suited to the GLO-Root
413 system because, like Arabidopsis, its small size allows mature root systems to be studied in
414 relatively small soil volumes^{29,30}. *LUC2o* driven by the *ZmUb1* promoter was introduced into
415 Brachypodium using the pANIC vector³¹. Brachypodium roots showed a distinct architec-
416 ture from Arabidopsis marked by prolific development of secondary and tertiary lateral roots
417 (Fig 8A). This is consistent with other studies that show that Brachypodium has a typical
418 grass root system³⁰. Comparison of root system development in rhizotrons with gel-based
419 media showed that root growth is higher in soil than in plates (Figure 8-figure supplement
420 1). Previous work has suggested that auxin levels in Brachypodium roots is sub-optimal for
421 growth³². Pacheco-Villalobos and colleagues suggest that, in Brachypodium, and contrary
422 to what happens in Arabidopsis, ethylene represses *YUCCA* reducing the synthesis of auxin.
423 The reduced growth that we observe in plates and the high levels of ethylene that build up
424 in sealed plates³³ would support this mechanism.

425 Tomato plants were transformed with *Pro35S:PPyRE8o* and *ProeDR5rev:LUC2* reporters.
426 The plants showed more rapid growth than Arabidopsis or Brachypodium and required
427 fertilizer to prevent obvious signs of stress (reduced growth, anthocyanin accumulation).
428 Root systems were imaged from 17 DAS plants. Roots showed presumptive lateral root
429 primordia marked by DR5-expression (Fig 8C-D). These results show that the GLO-Roots
430 method can be applied to study root systems of plants and will likely be useful for studying

⁴³¹ root systems of other small to medium sized model plants and for early stages of larger crop
⁴³² plants.

⁴³³ **Discussion.**

⁴³⁴ **GLO-Roots enables a multi-dimensional understanding of root biology.**

⁴³⁵ Recent studies of root systems has emphasized structural attributes as important contrib-
⁴³⁶ utors of root system function. Indeed, studies examining the role of genetic variants in
⁴³⁷ tolerating abiotic stress have demonstrated the importance of such characteristics⁸. Roots,
⁴³⁸ however, are highly diverse in the biology they perform and a multi-dimensional understand-
⁴³⁹ ing of root systems, which incorporates differences in signaling, metabolism and microbial
⁴⁴⁰ association as well as structure, may provide a clearer understanding of the degree to which
⁴⁴¹ sub-functionalization of the root system plays a role in important processes such as acclima-
⁴⁴² tion and efficient resource acquisition.

⁴⁴³ We have developed tools in GLO-Roots that allow for tracking multiple aspects of soil
⁴⁴⁴ physicochemical properties and root biology simultaneously. Using GLO-Roots, we are able
⁴⁴⁵ to map in 2D coordinates soil physical properties such soil moisture together with root ar-
⁴⁴⁶ chitecture traits such as directionality, growth rates and gene expression levels. All this
⁴⁴⁷ information is aggregated in layers for each x, y coordinate. Using GLO-RIA we integrate
⁴⁴⁸ this multilayer information, leveraging our ability to simultaneously and seamlessly investi-
⁴⁴⁹ gate root responses to environmental stimuli such as soil moisture content. Luciferases that
⁴⁵⁰ emit light at different wavelengths allow for constitutive and regulated promoters to be stud-
⁴⁵¹ ied together. Introduction of luciferase reporters into microbes provides an additional layer
⁴⁵² of information that provides a readout on the association between organisms and how this
⁴⁵³ might be affected by environmental conditions. The flexibility of the GLO-Roots system may
⁴⁵⁴ enable additional dimensionality to our understanding of root biology. Other physical prop-
⁴⁵⁵ erties such as CO₂ or pH mapping in rhizotrons have already been enabled by using planar
⁴⁵⁶ optodes³⁴. It may be possible to engineer LUX-based reporters in microbes that are respon-

457 sive to extracellular metabolites, creating microbial biosensors, and integration of such tools
458 may enable root-exudation and nutrition to be analyzed in soil. Split-Luciferase reporters
459 have been engineered that allow bi-molecular interactions to be studied. Finally, molecular
460 sensors analogous to FRET sensors, termed BRET-sensors³⁵, may allow metabolite tracking
461 dynamically through the root system. With additional innovation in the development of
462 luciferase reporters, the GLO-Roots systems will likely expand the repertoire of biological
463 processes that can be studied over an expanded range of developmental time points and
464 environmental conditions.

465 **Enhanced root growth and gravitropism may constitute an avoidance mechanism
466 used during water deficit stress.**

467 It has been proposed that plants with steep root systems will be better able to tap into deep
468 water resources and thus perform better under water deprivation. For example in rice, the
469 IR64 paddy cultivar shows shallow root systems in upland fields whereas Kinandang Patong,
470 an upland cultivar, is deeper rooting⁸. Plants maintain a number of regulatory pathways that
471 mediate changes in physiology during WD. Enhanced growth of root systems has been well
472 characterized in field-grown plants; however this has not been recapitulated in studies of gel-
473 grown Arabidopsis plants. Thus, it has been unclear whether Arabidopsis simply responds
474 to WD differently. Our results here show that Arabidopsis does indeed maintain a classical
475 WD response that expands the root system and directs growth downward. Interestingly,
476 under our stress regime, we did not observe a significant decrease in the relative water
477 content of shoot tissues (Figure 6-figure supplement 5), suggesting that the changes in root
478 architecture were sufficient to provide access to deep water and prevent dehydration. Such
479 changes in root growth are likely regulated through systemic and local signaling that involve
480 auxin signaling but acts independently of known pathways that control moisture-directed
481 root growth.

482 **Perspectives and Conclusions.**

483 Understanding plant biology requires a sophisticated understanding of how environmental
484 stimuli affect the form and function of plants as well as an understanding of how physiological
485 context informs such responses. Environmental conditions are at least as complex as the
486 plants they affect. Plant roots are exposed to a variety of environmental signals that change
487 in time and space at very different scales that are integrated at the whole plant system. It is
488 an important challenge in biology to develop methods of growing and studying plants that
489 present such stimuli in a manner that the plant is likely to encounter in nature. After all, the
490 plants we study have evolved to survive through mechanisms that have been selected, over
491 evolutionary time, in nature. It will be interesting for future studies to determine how other
492 environmental stimuli affect root growth using GLO-Roots and whether these responses
493 differ between accessions of Arabidopsis. Identification of the genetic loci responsible for
494 phenotypic variation in adult root phenotypes may identify the molecular basis for adaptive
495 variation that exists in this species and potentially identify loci that are useful for breeding
496 efforts needed for the next green revolution.

497 **Materials and methods.**

498 **Growth system.**

499 **Rhizotrons and growth system fabrication.** Rhizotrons are composed of two sheets of
500 1/8" abrasion resistant polycarbonate plastic (Makrolon AR (R)) cut to size using a water
501 jet (AquaJet LLC, Salem, OR), two acrylic spacers cut using a laser (Stanford Product
502 Realization Lab), two rubber U-channels cut to strips 30 cm long ([McMaster Carr part](#)
503 [# 8507K33](#)) and two sheets of black 0.030" thick polypropylene sheets ([McMaster Carr](#)
504 [part # 1451T21](#)) cut with a straight-edge razor blade. Rhizotron designs were drafted in
505 Adobe Illustrator (Adobe, San José, CA). The blueprints of all the parts are provided in
506 Supplement 1. The top edge of each polycarbonate sheet was painted with black 270 Stiletto
507 nail polish (Revlon, New York, NY).

508 **Boxes and holders.** Rhizotrons are held vertical during plant growth in a custom rack sys-
509 tem composed of two sheets of 1/4" black acrylic plastic cut with slots for eleven rhizotrons
510 using a laser, four 3/8" PVC rods ([McMaster Carr part # 98871a041](#)) secured with PVC
511 nuts ([McMaster Carr part # 94806a031](#)) to hold the acrylic sheets horizontal. The rack is
512 placed inside a 12" x 12" x 12" black polyethylene tank ([Plastic Mart part # R121212A](#)).

513 **Rhizotron preparation** The procedure to construct a rhizotron with soil is as follows:
514 Two pieces of polycarbonate plastic are laid flat on a table with the spacers inserted. Using
515 an electric paint gun, a fine mist of water is applied to the bare polycarbonate sheets. Then,
516 using a 2 mm sieve (US Standard Sieve Series N° 10) a fine layer of PRO-MIX(r) PGX soil
517 (Premier Tech, Canada) is applied. Excess soil is discarded by gently tapping the plastic
518 against the table in a vertical position. Water is sprayed again onto the soil, then a second
519 layer of Pro-MIX is applied as before. For P deficiency experiments soil supplemented with
520 1 ml of 100 µM P-Alumina (control) and 0-P-Alumina (P deficient) was used. To prevent
521 the soil from falling out of the bottom opening, a 3 x 6 cm piece of nylon mesh is rolled into
522 a 1 cm wide tube and placed at the bottom side of the rhizotron. The spacers are removed
523 and replaced by clean spacers. The two faces of the rhizotron are carefully joined together
524 and two rubber U-channels slipped on to clamp all pieces together. Assembled rhizotrons
525 are placed into the rack inside the boxes and 500 mL of water is added to the box.

526 **Plant growth** *Arabidopsis thaliana* seeds were stratified for 2 d at 4 °C in Eppendorf tubes
527 with distilled water. Seeds were suspended in 0.1 % agar and 5 to 10 were sown using
528 a transfer pipette in the rhizotron. A transparent acrylic sheet was mounted on top of
529 the box and sealed with tape to ensure high humidity conditions that enable *Arabidopsis*
530 germination. Three days after sowing, the cover was unsealed to decrease humidity and
531 allow the seedlings to acclimate to a dryer environment. From 3 days after sowing (DAS)
532 to the time the first true leaves emerged, it was critical to ensure that the top part of the
533 rhizotron remained humid for proper germination of the plants. Between three and five DAS
534 the rhizotrons were thinned leaving only the number plants required for that experiment,
535 typically one, except for experiments examining root-root interactions. Unless otherwise

536 stated, all the experiments presented here, treatments were started 10 DAS. Plants were
537 grown under long day conditions (16 h light / 8 h dark) using 20–22 °C (day/night) and
538 150 µE m⁻¹ s⁻¹. Two types of growth environments were used for experiments. A walk-in
539 growth chamber with fluorescent lightning and a growth cabinet with white LED lights.
540 Relative water content measurements were done as previously described³⁶

541 **qRT-PCR analysis.**

542 Seeds were surface sterilized as described before² and grown in rhizotrons, 100 cm³ pots, or
543 on two types of 1% agar (Duchefa) media containing either 1x MS nutrients (Caisson) and 1%
544 Sucrose, (termed ms media) or ¼x MS nutrients only (termed ms25 media). Both media were
545 buffered using 0.5 g/L MES and pH was adjusted to 5.7 with KOH. All plants were grown
546 together in a growth cabinet with LED lights under long day conditions (16h day/8h night).
547 Root and shoot tissue was collected separately from individual plants at the end of the day
548 (1 hour before the lights shut off) and at the end of the night (1 hour before lights came on).
549 Three biological replicates were collected for each condition. RNA was extracted using the
550 Plant RNA MiniPrepTM kit (ZYMO Research) according to manufacturer's instructions
551 with on-column DNase treatment (Qiagen). cDNA was made using the iScript Advanced
552 cDNA Synthesis for RT-qPCR kit (Bio-Rad) from 200 ng of total RNA. qRT-PCR was
553 performed using a Fluidigm BioMarkTM 96.96 Dynamic Array IFC with the EvaGreen®
554 (Bio-Rad) fluorescence probe according to the Fluidigm Advanced Development Protocol
555 number 37. For the analysis, all the reactions with no amplification ($C_t = 999$) were set to
556 the maximal C_t for that assay type. The two technical replicates were then averaged and
557 dC_t values calculated using AT3G07480, AT4G37830, At1g13320 and At1g13440 as reference
558 internal controls. PCA plots were generated with Devium Web³⁷ using dC_t values. dCT
559 values were calculated as $dCT = CT_{\text{gene interest}} - \text{mean}(CT_{\text{reference gene}})$. Primers
560 used are listed in file Supplement 8.

561 **Biological components.**

562 **Codon optimization of luciferases.** The following luciferases that emit light at different
563 wavelengths were codon optimized for Arabidopsis (Genscript, Piscataway, NJ): LUC2: a
564 yellow improved version (Promega, Madison, WI) of the original *Photinus pyralis* (firefly)
565 LUC.

- 566 • Ppy RE8: a red variant³⁸ of the *P. pyralis* thermostable variant Ppy RE-TS³⁹.
- 567 • CBG99: a green variant (Promega, Madison, WI) from yellow click beetle (*Pyrophorus*
568 *plagiophthalmus*) luciferases.
- 569 • CBR: a red variant (Promega, Madison, WI) from yellow click beetle.

570 **Non-optimized luciferases.** We also used the following non-optimized luciferases:

- 571 • nanoLUC: a blue luciferase isolated from a deep sea shrimp¹⁴.
- 572 • venusLUC2: a venus-LUC2 fusion reported to show higher luminescence output than
573 LUC2¹⁵.
- 574 • A transposon containing the bacterial luciferase-containing LUX operon was inte-
575 grated into the *Pseudomonas fluorescens* CH267²² genome by conjugation with *E.*
576 *coli* SM10 *pir* containing pUT-EM7-LUX⁴⁰ and used to track root microbe coloniza-
577 tion. For inoculation 9 DAS plants were inoculated with 2 mL of an overnight bacterial
578 culture resuspended in 10 mM MgSO₄ and diluted to 0.01 OD.

579 **Generation of single-reporter transgenic plants.** We generated transcriptional fu-
580 sions of all luciferases to constitutive promoters to examine the activity level and emission
581 spectrum of each isoform. The *attL1-attL2* entry clones containing plant-codon optimized
582 coding sequence of *LUC2*, *PpyRe8*, *CBG99* and *CBR* were synthesized by Genscript. A
583 DNA fragment including the *UBQ10* promoter region and first intron was amplified from
584 Col-0 genomic DNA with primers incorporating the attB1, attB4 combination sites at the 5'

585 and 3' respectively. The PCR product was then introduced into pDONR™ P4-P1R (Invitro-
586 gen) through a classic Gateway BP-reaction. The resulting plasmid, the *attL1-attL2* entry
587 clones with luciferase sequences, an empty *attR2-attL3** entry clone and the destination
588 vector dpGreenmCherry² were used to construct *ProUBQ10:LUC2o*, *ProUBQ10:PpyRE8o*,
589 *ProUBQ10:CBG99o* and *ProUBQ10:CBrO* through Gateway LR reactions. The destination
590 vector *dpGreenmCherry* contains a plasma membrane-localized mCherry coding sequence
591 driven by the 35S promoter and is used as a selectable marker of transformation at the
592 mature seed stage². We used Golden Gate cloning and the destination vectors that we had
593 generated before¹⁶ for the following fusions: *ProUBQ10:nanoLUC2*, *ProUBQ10:venusLUC*,
594 *ProACT2:PpyRE8o*. Briefly, the different components of each construct were PCR ampli-
595 fied with complementary BsaI or SapI cutting sites, mixed with the destination vector in
596 a single tube, digested with either BsaI or SapI, ligated with T4 DNA ligase, then trans-
597 formed into E. coli Top10 cells and plated on LB antibiotic plates containing X-gal as pre-
598 viously described¹⁶. Junction sites were confirmed by sequencing. We used pSE7 (Addgene
599 ID #: pGoldenGate-SE7: 47676) as the destination vector of the *ProUBQ10:nanoLUC2*,
600 *ProUBQ10:venusLUC* constructs and pMYC2 (Addgene ID #: pGoldenGate-MCY2: 47679)
601 as the destination vector for *ProACT2:PpyRE8o*. Maps of all the vectors can be found in
602 Supplement 8. *ProUBQ10:LUC2o* was transformed into Col-0, Bay and Sha accessions, the
603 *tir1-1*⁴¹ mutant and the *miz1*⁴² T-DNA insertion line (SALK_126928).

604 **Brachypodium distachyon.** The Arabidopsis plant-codon optimized Luciferase gene,
605 *LUC2o*, was inserted into the monocot vector pANIC10 via Gateway cloning³¹. *Brachy-
606 podium distachyon* plants were transformed using the method of Vogel and Hill⁴³.

607 **Tomato.** The transcriptional fusion *ProeDR5:LUC2* was generated by cloning the
608 *ProeDR5:LUC2* DNA fragment into the pBIB expression vector via restriction sites SalI
609 and Acc65I. The eDR5 promoter is an enhanced version of DR5 containing 13 repeats of
610 the 11-nucleotide core DR5 element⁴⁴ and the pBIB expression vector contains an NPTII
611 resistance gene under the control of the NOS promoter for use as a selectable marker during

612 transformation. All tomato transformations were performed by the Ralph M. Parsons
613 Foundation Plant Transformation Facility (University of California, Davis).

614 **Generation of dual-reporter plants.** To generate dual-reporter plants expressing lu-
615 ciferase isoforms that emit light with divergent emission spectra we used *ProACT2:PpyRE8o*
616 as the root structural marker and ZAT12:LUC²¹ and DR5:LUC+²⁰ lines that were trans-
617 formed with the *ProACT2:PpyRE8o* construct. All constructs were transformed using a
618 modified floral dip method as described in².

619 To make the dual color tomato plants, the *Pro35S:PpyRE8o* transcriptional fusion was
620 generated by putting the plant-codon optimized coding sequence described above into the
621 pMDC32 expression vector through a Gateway LR reaction. The pMDC32 vector con-
622 tains a hygromycin resistance gene under the control of the 35S promoter for use as a se-
623 lectable marker during transformation. This construct was transformed into the transgenic
624 *ProeDR5:LUC2* tomato line.

625 **In vivo emission spectra of plants constitutively expressing luciferase isoforms.**
626 To generate *in vivo* emission spectra of all constitutively expressed luciferases, seeds were
627 sterilized and sown on MS plates as described before². After 8 days, seedlings were treated
628 with a 100 µM luciferin solution, incubated at room temperature for 3 hours and imaged
629 using an IVIS Spectrum imaging system (Perkin Elmer, Waltham , MA) using 20 nm band-
630 pass emission filters at the following wavelengths (in nm: 490-510, 510-530, 530-550, 550-570,
631 570-590, 590-610, 610-630, 630-650, 650-670, 670-690, 690-710). Raw images were analyzed
632 using Fiji and *in vivo* emission spectra were constructed. The full emission spectra of LUX
633 and nanoLUC could not be constructed since the maximum of these two luciferases is below
634 the lower band pass filter that were available.

635 **Imaging system.** We designed a custom imaging system (GLO1, Growth and Lumines-
636 cence Observatory 1) optimized for imaging dual-reporter luciferase expression in our custom
637 rhizotrons. The design was a joint effort with Bioimaging Solutions (San Diego, CA) who

638 also built the system and wrote the acquisition software that drives all the mechanical parts
639 of the system. The system is composed by two 2048 x 2048 PIXIS-XB cameras (Princeton
640 Instruments, Trenton, NJ) mounted on top of each other to capture two fields of view en-
641 compassing approximately two 15 x 15 cm areas corresponding to the top or bottom of the
642 rhizotron. The cameras are fitted with a Carl-Zeiss macro lens. A filter wheel with space
643 for four, 76.2 mm filters is positioned in front of the cameras and controlled by a stepper
644 motor allowing for automated changing of the filter wheel position. We used two -542/50
645 and 450/70- custom cut Brightline(R) band-pass filters (Semrock, Rochester, NY). In sin-
646 gle color imaging mode, the filter wheel is operated without filters. Positioned in front of
647 the filter wheel is a removable rhizotron holder mounted on a stepper motor. This stepper
648 motor is also controlled by the GLO-1 software allowing automatic acquisition of images
649 from both sides of the rhizotron sequentially. The whole imaging system is enclosed in a
650 light-tight black box with a door that allows loading and un-loading of rhizotrons.

651 **Plant Imaging.** Around 50 mL of 300 μ M D-luciferin (Biosynth, Itasca, IL) was added
652 to soil at the top of the rhizotron. In general 5 min exposures were taken per rhizotron, per
653 side, per channel. For daily imaging experiments, plants were imaged at dawn (+/- 1 hr)
654 to reduce possible effects on diurnal rhythms of keeping plants in the dark during imaging.
655 Shoot images were taken using a Nikon D3100 camera.

656 **Image Preparation.** Four individual images are collected: top front, bottom front, top
657 back and bottom back. Using an automated [ImageJ macro](#), a composite image is generated
658 as follows: 1)To correct for differences in background values between the two cameras the
659 mean background value of each image is subtracted from 200; 2) images are rotated and
660 translated to control for small misalignments between the two cameras; 3) the top and
661 bottom images of each side are merged; 4) the back image is flipped horizontally; 5) the
662 front and back images are combined using the maximum values. When dual color images are
663 acquired this operation is repeated for each channel. The final images produced are 16-bit
664 depth and 4096 x 2048 pixels. The scale of the images is 138.6 pixels per cm. Considering

665 that an Arabidopsis roots is 100 μm this results in 1.39 pixels across an Arabidopsis root.

666 **GLO-RIA imageJ plug-in.** GLO-RIA uses a combination of existing tools to extract
667 relevant root architecture features. Directionality is acquired using the [directionality plugin](#)
668 from ImageJ. After the number of direction bins (we usually use bins of 2°) is defined by the
669 user, a 5x5 sobel operator is used to derive the local gradient orientation. This orientation
670 is then used to build a distribution of directions by assigning the square of the orientation
671 into the appropriate bin. Instead of representing the total counts at each orientation a
672 relative value is calculated by dividing the individual values at each bin by the total sum
673 of the histogram (and multiplying by 100). Similar algorithms have been used to quantify
674 dynamic changes in the plant cytoskeleton⁴⁵.

675 The Elliptic Fourier Descriptors are aquired using the [Fourier Shape Analysis plugin](#) on con-
676 vex hull shape of the root system. Elliptic Fourier Descriptors have been used in numerous
677 studies to analyse variations in shapes, notably in leaves (e.g⁴⁶).

678 The shape analysis is inspired by RootScape¹⁷. Due to the absence of fixed, recognisable
679 structures in root system (that are required for the position of true landmarks), pseudo-
680 landmarks are automatically extracted from the root systems. Shortly, the image is divided
681 vertically at equidistant positions (with the number defined by the user) and for each of the
682 image stripes, the minimum and maximum x coordinates are computed. The shape analy-
683 sis is therefore able to discriminate root system with different vertical root distributions or
684 global root system orientation (e.g. chemotropism) . The code source for the plugin, manual
685 and sample images can be found in the [github repository](#) of the project.

686 Statistical analysis was performed in R⁴⁸. The tidyR⁴⁹, dplyr⁴⁹, gridExtra⁵⁰, shapes⁵¹,
687 geomorph⁵², ggplot2⁵³ and cowplot⁵⁴ packages were used for data preparation, analysis
688 and plotting. Final figure preparation was done in [Inkscape](#).

689 **Data availability.** All the scripts and original data used to analyze and produce the
690 images can be accessed in the Github repository of the project: github.com/rr-lab/GLO-
691 Roots. Raw files of all the images used in the paper are available in [Dryad](#).

692 Acknowledgements.

693 Work in the lab of JRD was funded by the Carnegie Institution for Science Endowment
694 and grants from the National Science Foundation (MCB-115795) and Department of En-
695 ergy, Biological and Environmental Research program (DE-SC0008769). RRA was sup-
696 ported by a Carnegie Postdoc Fellowship and currently by Conacyt Ciencia Básica Joven
697 Investigador grant number (CB-2014-01-238101). GL was supported by the Belgian Fonds
698 de la Recherche Scientifique. JM was funded by the National Science Foundation (IOS-
699 0820854). CH is funded by MGH Toteston & Fund for Medical Discovery Fellowship grant
700 2014A051303 and NIH R37 grant GM48707 and NSF grant MCB-0519898 awarded to Fred-
701 erick Ausubel, and previously by the Gordon and Betty Moore Foundation through Grant
702 GBMF 2550.01 from the Life Sciences Research Foundation. JV was funded by the Office
703 of Biological and Environmental Research, Office of Science, US Department of Energy, in-
704 teragency agreements DE-SC0001526 and DE-AI02-07ER64452. We thank Robert Mittler
705 and Philip Benfey for providing seeds of ZAT12:LUC and DR5:LUC+ respectively.
706 We also thank Neil Robbins and members of the Dinneny lab for critical review of the
707 manuscript and suggestions during the development of the project. We greatly appreciate
708 Tim Doyle at the Stanford Small Animal Imaging Facility for providing advice in the use of
709 luciferase-based imaging approaches.

710 Competing interests.

711 We do not have any competing interests that we are aware of.

955 **References**

- 956 1.Dinneny, J. R. *et al.* Cell identity mediates the response of *Arabidopsis* roots to abiotic
957 stress. *Science* **320**, 942–945 (2008).
- 958 2.Duan, L. *et al.* Endodermal ABA Signaling Promotes Lateral Root Quiescence during
959 Salt Stress in Arabidopsis Seedlings. *Plant Cell* **25**, 324–341 (2013).
- 960 3.Lynch, J. P. & Wojciechowski, T. Opportunities and challenges in the subsoil: pathways
961 to deeper rooted crops. *J. Exp. Bot.* **66**, 2199–2210 (2015).
- 962 4.Brady, N. C. & Weil, R. R. *Elements of the nature and properties of soils*. (Prentice Hall,
963 2009).
- 964 5.Bao, Y. *et al.* Plant roots use a patterning mechanism to position lateral root branches
965 toward available water. *Proc Natl Acad Sci* **111**, 9319–9324 (2014).
- 966 6.Tabata, R. *et al.* Perception of root-derived peptides by shoot LRR-RKs mediates systemic
967 N-demand signaling. *Science* **346**, 343–346 (2014).
- 968 7.Rosquete, M. R. *et al.* An Auxin Transport Mechanism Restricts Positive Orthogravit-
969 ropicism in Lateral Roots. *Current Biology* **23**, 817–822 (2013).
- 970 8.Uga, Y. *et al.* Control of root system architecture by DEEPER ROOTING 1 increases
971 rice yield under drought conditions. *Nat. Genet.* **45**, 1097–1102 (2013).
- 972 9.Postma, J. A. & Lynch, J. P. The optimal lateral root branching density for maize depends
973 on nitrogen and phosphorus availability. *Plant Physiol.* **166**, 590–602 (2014).
- 974 10.Laliberté, E. *et al.* How does pedogenesis drive plant diversity? *Trends in ecology &*
975 *evolution* **28**, 331–340 (2013).
- 976 11.Tian, H., De Smet, I. & Ding, Z. Shaping a root system: regulating lateral versus primary
977 root growth. *Trends in plant science* **19**, 426–431 (2014).
- 978 12.Schneider, C. A., Rasband, W. S. & Eliceiri, K. W. NIH Image to ImageJ: 25 years of
979 image analysis. *Nature methods* **9**, 671–675 (2012).

- 980 13.Meijon, M., Satbhai, S. B., Tsuchimatsu, T. & Busch, W. Genome-wide association study
981 using cellular traits identifies a new regulator of root development in. *Nat. Genet.* **46**, 77–81
982 (2013).
- 983 14.Hall, M. P. *et al.* Engineered Luciferase Reporter from a Deep Sea Shrimp Utilizing a
984 Novel Imidazopyrazinone Substrate. *ACS chemical biology* **7**, 1848–1857 (2012).
- 985 15.Hara-Miyauchi, C. *et al.* Bioluminescent system for dynamic imaging of cell and animal
986 behavior. *Biochem. Biophys. Res. Commun.* **419**, 188–193 (2012).
- 987 16.Emami, S., Yee, M.-C. & Dinneny, J. R. A robust family of Golden Gate Agrobacterium
988 vectors for plant synthetic biology. *Front. Plant Sc.* **4**, 339 (2013).
- 989 17.Ristova, D. *et al.* RootScape: a landmark-based system for rapid screening of root
990 architecture in Arabidopsis. *Plant Physiology* **161**, 1086–1096 (2013).
- 991 18.Lobet, G. *et al.* Root System Markup Language: toward a unified root architecture
992 description language. *Plant Physiol.* **167**, 617–627 (2015).
- 993 19.Pagès, L. *et al.* Calibration and evaluation of ArchiSimple, a simple model of root system
994 architecture. *Ecological Modelling* **290**, 76–84 (2014).
- 995 20.Moreno-Risueno, M. A. *et al.* Oscillating gene expression determines competence for
996 periodic *Arabidopsis* root branching. *Science* **329**, 1306–1311 (2010).
- 997 21.Miller, G. *et al.* The plant NADPH oxidase RBOHD mediates rapid systemic signaling
998 in response to diverse stimuli. *Science Signaling* **2**, ra45 (2009).
- 999 22.Haney, C. H., Samuel, B. S., Bush, J. & Ausubel, F. M. Associations with rhizosphere
1000 bacteria can confer an adaptive advantage to plants. *Nature Plants* **1**, 15051 (2015).
- 1001 23.Mandoli, D. F., FORD, G. A., WALDRON, L. J., NEMSON, J. A. & Briggs, W. R. Some
1002 spectral properties of several soil types: implications for photomorphogenesis*. *Plant Cell*
1003 *Environ.* **13**, 287–294 (1990).
- 1004 24.Galen, C., Rabenold, J. J. & Liscum, E. Functional ecology of a blue light photoreceptor:
1005 effects of phototropin-1 on root growth enhance drought tolerance in *Arabidopsis thaliana*.

- ¹⁰⁰⁶ 25.Moni, A., Lee, A. Y., Briggs, W. R. & Han, I. S. The blue light receptor Phototropin 1
¹⁰⁰⁷ suppresses lateral root growth by controlling cell elongation. *Plant Biology* 34–40 (2014).
- ¹⁰⁰⁹ 26.Yokawa, K., Kagenishi, T. & Baluška, F. Root photomorphogenesis in laboratory-
¹⁰¹⁰ maintained Arabidopsis seedlings. *Trends Plant Sci.* **18**, 117–119 (2013).
- ¹⁰¹¹ 27.Lobell, D. B. *et al.* Greater Sensitivity to Drought Accompanies Maize Yield Increase in
¹⁰¹² the U.S. Midwest. *Science* **344**, 516–519 (2014).
- ¹⁰¹³ 28.Ort, D. R. & Long, S. P. Limits on Yields in the Corn Belt. *Science* **344**, 484–485 (2014).
- ¹⁰¹⁴ 29.Pacheco-Villalobos, D. & Hardtke, C. S. Natural genetic variation of root system archi-
¹⁰¹⁵ tecture from Arabidopsis to Brachypodium: towards adaptive value. *Philosophical Trans-
1016 actions of the Royal Society of London B: Biological Sciences* **367**, 1552–1558 (2012).
- ¹⁰¹⁷ 30.Watt, M., Schneebeli, K., Dong, P. & Wilson, I. W. The shoot and root growth of
¹⁰¹⁸ Brachypodium and its potential as a model for wheat and other cereal crops. *Functional
1019 Plant Biol.* **36**, 960–969 (2009).
- ¹⁰²⁰ 31.Mann, D. G. J. *et al.* Gateway-compatible vectors for high-throughput gene functional
¹⁰²¹ analysis in switchgrass (*Panicum virgatum* L.) and other monocot species. *Plant Biotechnol.
1022 J.* **10**, 226–236 (2012).
- ¹⁰²³ 32.Pacheco-Villalobos, D., Sankar, M., Ljung, K. & Hardtke, C. S. Disturbed Local
¹⁰²⁴ Auxin Homeostasis Enhances Cellular Anisotropy and Reveals Alternative Wiring of
¹⁰²⁵ Auxin-ethylene Crosstalk in Brachypodium distachyon Seminal Roots. *PLoS Genet* **9**,
¹⁰²⁶ e1003564 (2013).
- ¹⁰²⁷ 33.Buer, C. S., Wasteneys, G. O. & Masle, J. Ethylene modulates root-wave responses in
¹⁰²⁸ Arabidopsis. *Plant Physiology* **132**, 1085–1096 (2003).
- ¹⁰²⁹ 34.Blossfeld, S., Schreiber, C. M., Liebsch, G., Kuhn, A. J. & Hinsinger, P. Quantitative
¹⁰³⁰ imaging of rhizosphere pH and CO₂ dynamics with planar optodes. *Annals of Botany* **112**,
¹⁰³¹ 267–276 (2013).

- 1032 35.Shaw, S. L. & Ehrhardt, D. W. Smaller, Faster, Brighter: Advances in Optical Imaging
1033 of Living Plant Cells. *Annu. Rev. Plant Biol.* **64**, 351–375 (2013).
- 1034 36.Barr, H. & Weatherley, P. A re-examination of the relative turgidity technique for esti-
1035 mating water deficit in leaves. *Aust. J. Biol. Sci* **15**, 413–428 (1962).
- 1036 37.Grapov, D. DeviumWeb: Dynamic Multivariate Data Analysis and Visualization Plat-
1037 form.
- 1038 38.Branchini, B. R. *et al.* Red-emitting luciferases for bioluminescence reporter and imaging
1039 applications. *Analytical Biochemistry* **396**, 290–297 (2010).
- 1040 39.Branchini, B. R. *et al.* Thermostable red and green light-producing firefly luciferase
1041 mutants for bioluminescent reporter applications. *Analytical Biochemistry* **361**, 253–262
1042 (2007).
- 1043 40.Lane, M. C., Alteri, C. J., Smith, S. N. & Mobley, H. L. T. Expression of flagella is
1044 coincident with uropathogenic Escherichia coli ascension to the upper urinary tract. *Proc.
1045 Natl. Acad. Sci. U.S.A.* **104**, 16669–16674 (2007).
- 1046 41.Ruegger, M. *et al.* The TIR1 protein of Arabidopsis functions in auxin response and is
1047 related to human SKP2 and yeast grr1p. *Genes Dev* **12**, 198–207 (1998).
- 1048 42.Moriwaki, T. *et al.* Hormonal Regulation of Lateral Root Development in Arabidopsis
1049 Modulated by MIZ1 and Requirement of GNOM Activity for MIZ1 Function. *Plant Physiol.*
1050 **157**, 1209–1220 (2011).
- 1051 43.Vogel, J. & Hill, T. High-efficiency Agrobacterium-mediated transformation of Brachy-
1052 podium distachyon inbred line Bd21-3. *Plant Cell Rep* **27**, 471–478 (2008).
- 1053 44.Covington, M. F. & Harmer, S. L. The Circadian Clock Regulates Auxin Signaling and
1054 Responses in Arabidopsis. *Plos Biol* **5**, e222 (2007).
- 1055 45.Lindeboom, J. J. *et al.* A Mechanism for Reorientation of Cortical Microtubule Arrays
1056 Driven by Microtubule Severing. *Science* **342**, 1245533–1–1245533–11 (2013).

- 1057 46.Chitwood, D. H. *et al.* A modern ampelography: a genetic basis for leaf shape and
1058 venation patterning in grape. *Plant Physiology* **164**, 259–272 (2014).
- 1059 47.Iwata, H. & Ukai, Y. SHAPE: a computer program package for quantitative evaluation of
1060 biological shapes based on elliptic Fourier descriptors. *The Journal of Heredity* **93**, 384–385
1061 (2002).
- 1062 48.R Core Team. *R: A language and environment for statistical computing*. (R Foundation
1063 for Statistical Computing, 2014). at <<http://www.R-project.org/>>
- 1064 49.Wickham, H. *Tidyr: Easily tidy data with spread() and gather() functions*. (2014). at
1065 <<http://CRAN.R-project.org/package=tidyr>>
- 1066 50.Auguie, B. *GridExtra: Functions in grid graphics*. (2012). at <<http://CRAN.R-project.org/>>/
1067 [package=gridExtra](http://CRAN.R-project.org/package=gridExtra)>
- 1068 51.Dryden, I. L. *Shapes: Statistical shape analysis*. (2013). at <<http://CRAN.R-project.org/>>/
1069 [package=shapes](http://CRAN.R-project.org/package=shapes)>
- 1070 52.Adams, D. & Otarola-Castillo, E. Geomorph: An r package for the collection and analysis
1071 of geometric morphometric shape data. *Methods in Ecology and Evolution* **4**, 393–399 (2013).
- 1072 53.Wickham, H. *Ggplot2: Elegant graphics for data analysis*. (Springer New York, 2009).
1073 at <<http://had.co.nz/ggplot2/book>>
- 1074 54.Wilke, C. O. *cowplot: Streamlined Plot Theme and Plot Annotations for ggplot2*. (2015).
1075 at <<http://cran.r-project.org/web/packages/cowplot/index.html>>

₇₁₂ **Tables.**

₇₁₃ **Table 1:** Luciferases used in this study.

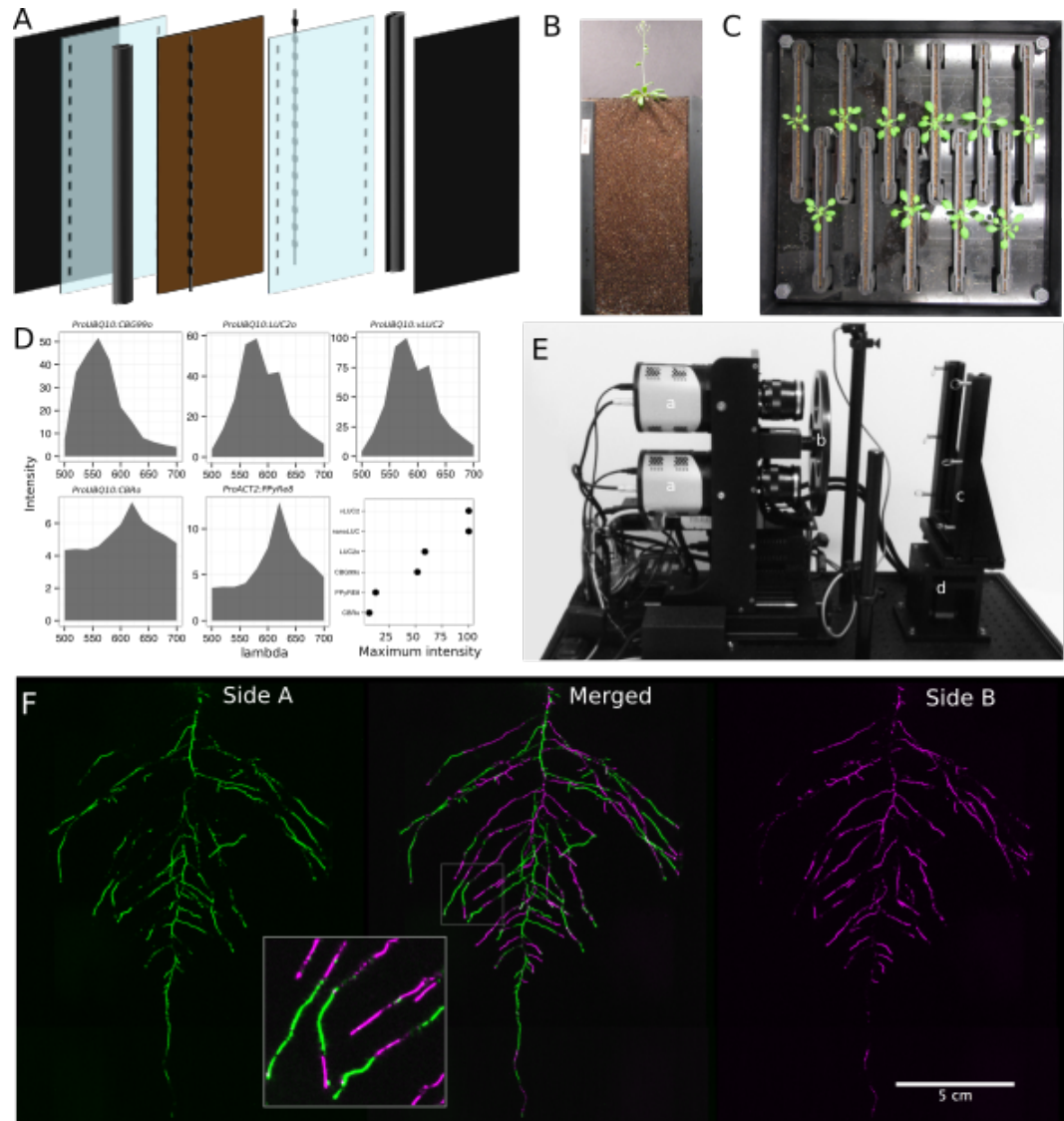
Luciferase	Origin	maximum wavelength	Substrate
Ppy RE8	firefly	618	D-luciferin
CBGRed	click beetle	615	D-luciferin
venus-LUC2	FP + firefly	580	D-luciferin
LUC(+)	firefly	578	D-luciferin
CBG99	click beetle	537	D-luciferin
lux operon	A. fischeri	490	biosynthesis pathway encoded within operon
nanoLUC	Deep sea shrimp	470	furimazine

₇₁₄ **Table 2:** list of root system features extracted using GLO-RIA.

variable	unit
projected area	cm ²
number of visible roots	-
depth	cm
width	cm
convex hull area	cm ²
width	cm
feret	cm
feret angle	°
circularity	-
roundness	-
solidity	-
center of mass	cm
Directionality	°
Euclidean Fourier Descriptors	-

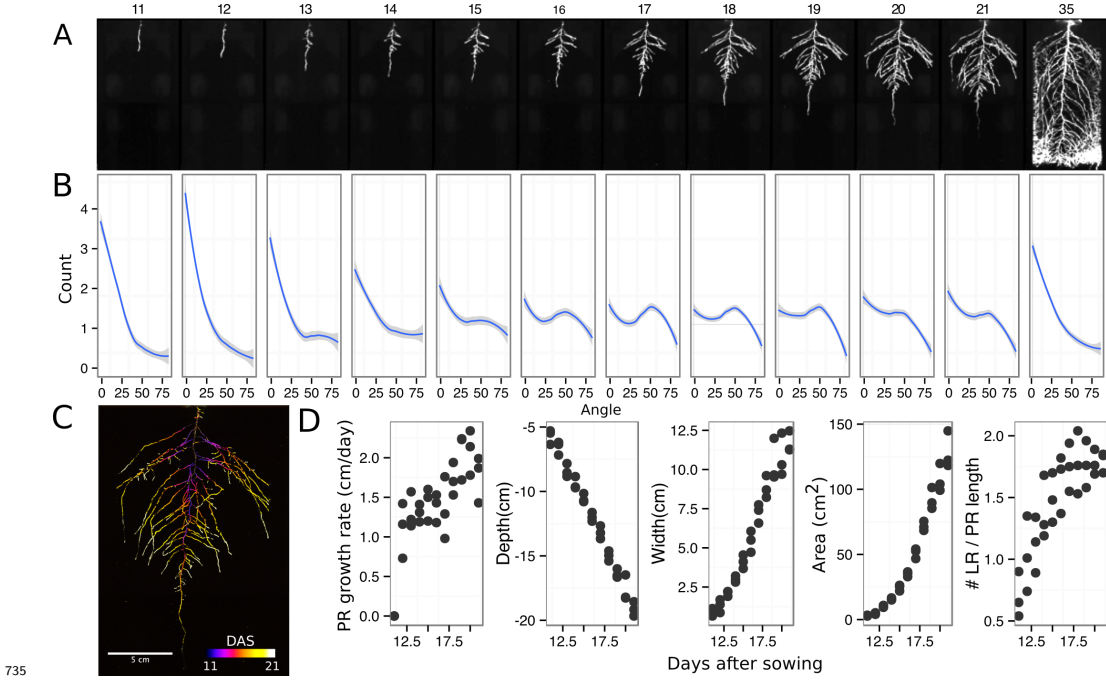
variable	unit
Pseudo landmarks	-

715 **Figures**

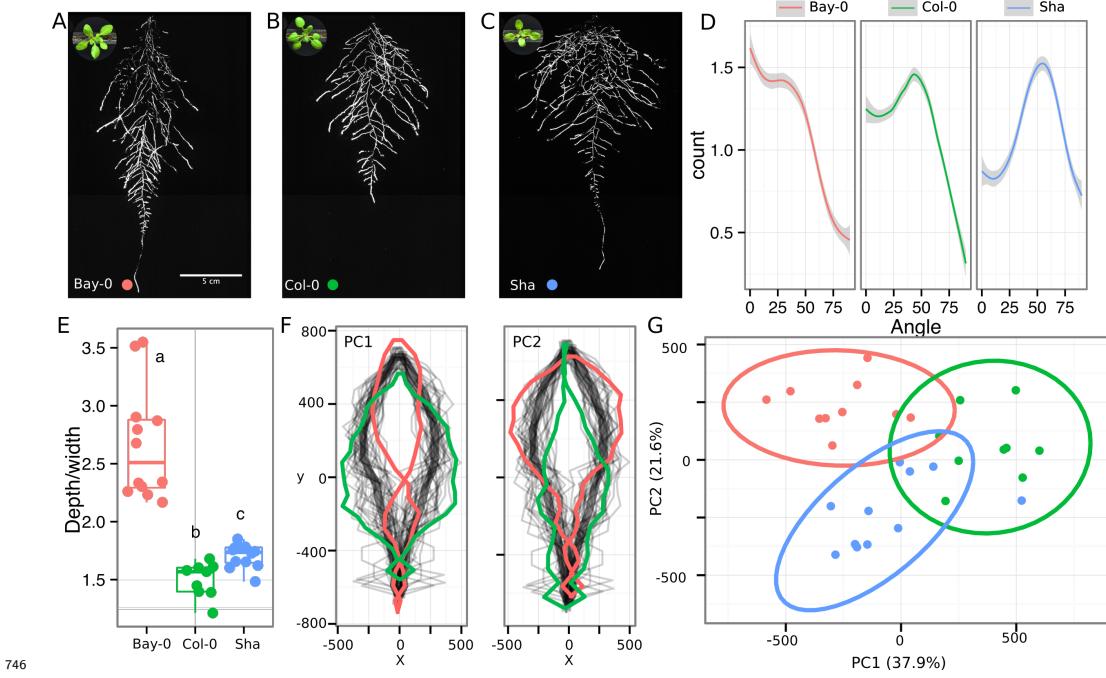


716
717 **Figure 1. GLO-Roots growth and imaging systems** A) 3D representation of the
718 different physical components of the rhizotron: plastic covers, polycarbonate sheets,
719 spacers and rubber U-channels. Blueprints are provided in Supplementary material 1. In brown,
720 soil layer. B) Thirty five day-old plant in rhizotron with black covers removed. C) Top view
721 of holding box with eleven rhizotrons. D)In vivo emission spectra of different luciferases
722 used in this study. Transgenic homozygous lines expressing the indicated transgenes were

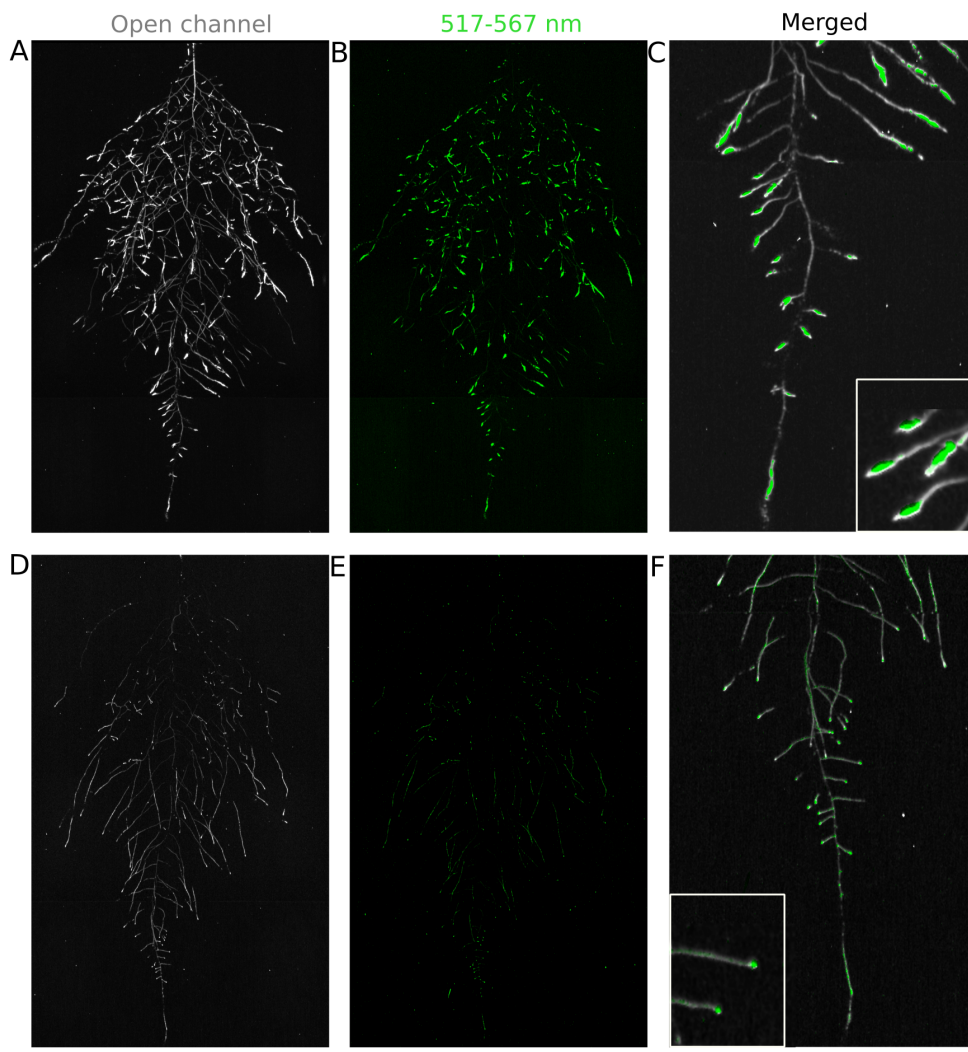
723 grown on agar media for 8 days. Luciferin (300 μ M) was sprayed on the seedlings and
724 plates were kept in the dark and then imaged for 2 s at wavelengths ranging from 500
725 to 700 nm. Five intensity values were taken from different parts of the roots of different
726 seedlings and averaged. Relative maximum intensity values are indicated in the lower right
727 graph. E) GLO 1 imaging system. The system is composed by two back illuminated CCD
728 cameras (a) cooled down to -55 °C. A filter wheel (b) allows for spectral separation of the
729 different luciferases. On the right, a rhizotron holder (c) is used to position the rhizotrons
730 in front of the cameras. A stepper motor (d) rotates the rhizotron 180° to image both
731 sides. F) A 21 DAS plant expressing *ProUBQ10:LUC2o* was imaged on each of two sides
732 of the rhizotron; luminescence signal is colorized in green or magenta to indicate side. In
733 the middle of the panel, a combined image of the two sides is shown. The inset shows a
734 magnified part of the root system. FW: fresh weight, PR: Primary root.



736 **Figure 2. Time-lapse imaging of root systems and quantification using GLO-**
 737 **RIA.** A) Typical daily time-lapse image series from 11 to 35 DAS of a *ProUBQ10:LUC2o*
 738 Col-0 plant. B) Directionality of the root system of plants in panel A calculated using the
 739 directionality plugin implemented in GLO-RIA. C) Color coded projection of root growth
 740 using the images in panel A. D) Primary root growth rate, depth, width, root system area
 741 are automatically calculated from the convex hull, which is semi-automatically determined
 742 with GLO-RIA. Lateral root number and number of lateral roots divided by the primary
 743 root length were quantified manually. A Local Polynomial Regression Fitting with 95%
 744 confidence interval (grey) was used to represent the directionality distribution curve. (0° is
 745 the direction of the gravity vector).



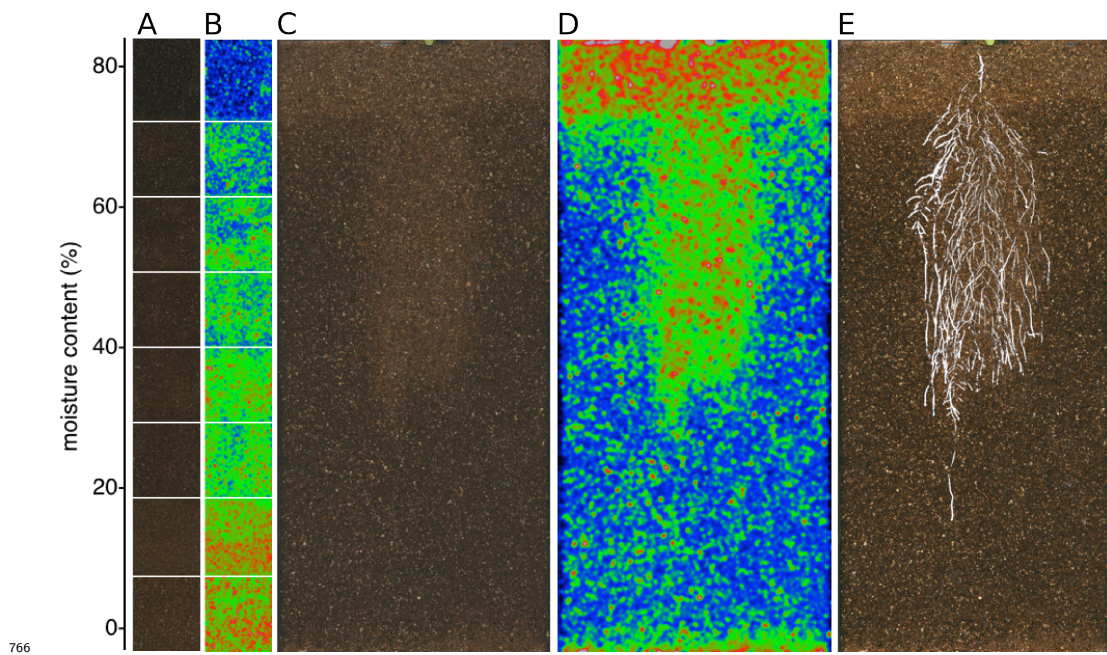
747 **Figure 3. Variation in root architecture between accessions of *Arabidopsis*.** Rep-
 748 resentative root and shoot images of A) Bay-0, B) Col-0 and C) Sha accessions transformed
 749 with *_ProUBQ10:LUC2o_* and imaged after 22 DAS. D) Directionality of the root systems,
 750 E) depth/width ratio, F) Pseudo-landmarks describing shape variation in root system archi-
 751 tecture. Eigenvalues derived from the analysis of 9-12 plants per accession is shown. The
 752 first two Principal Components explaining 38% (PC1) and 22% (PC2) of the shape variation
 753 are plotted. PC1 captures homogeneity of root system width along the vertical axis and
 754 PC2 a combination of depth and width in top parts of the root system. Red and green
 755 lines indicate -3SD and +3SD (Standard Deviations), respectively G) PC separation of the
 756 different ecotypes using the PCs described in (F). A Local Polynomial Regression Fitting
 757 with 95% confidence interval (grey) was used to represent the directionality distribution
 758 curve. 0° is the direction of the gravity vector. Wilcoxon test analysis with p < 0.01 was
 759 used to test significant differences between the different accession (n = 9-12 plants).



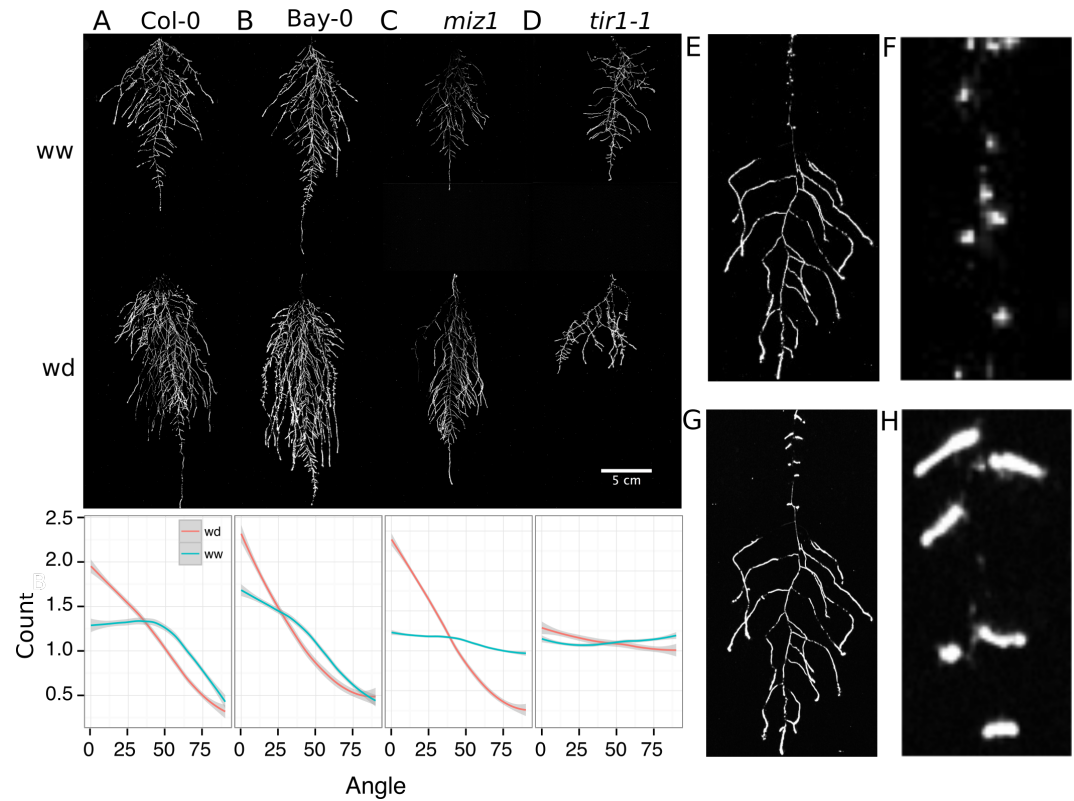
760

761 **Figure 4. Dual-color reporter visualization of structure and gene expression.**

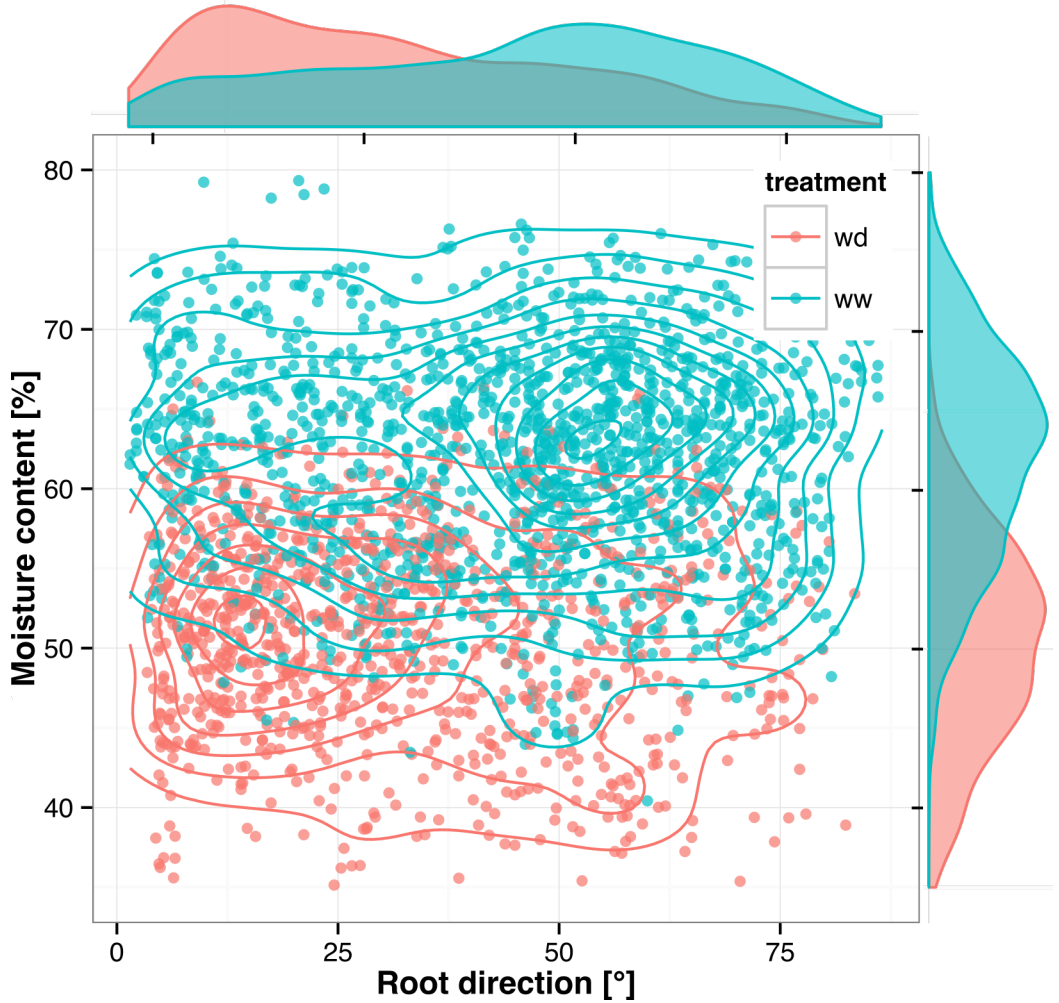
762 Images of whole root systems (A, D) or magnified portion of roots (C, F) at 22 DAS
 763 expressing *ProDR5rev:LUC+* (green, A, B) or *ProZAT12:LUC* signal (green, D, E) with
 764 skeletonized representation of roots generated using the *ProACT2:PpyRE8o* reporter
 765 expression (in grey).



766 **Figure 5. Soil moisture and root architecture mapping in rhizotrons.** A) Com-
 767 posite image showing regions of soil made from rhizotrons prepared with different moisture
 768 levels. B) Differences in grey-scale intensity values were enhanced using a 16-color Look
 769 Up Table (LUT). Brightfield image of soil in rhizotron (C) and converted using 16-color
 770 LUT to enhance visualization of distribution of moisture (D) . E) Root system of a Bay-0
 771 22 DAS and subjected to water deprivation since 13 DAS. Root system visualized using
 772 luminescence and overlaid on brightfield image of soil in (C).
 773

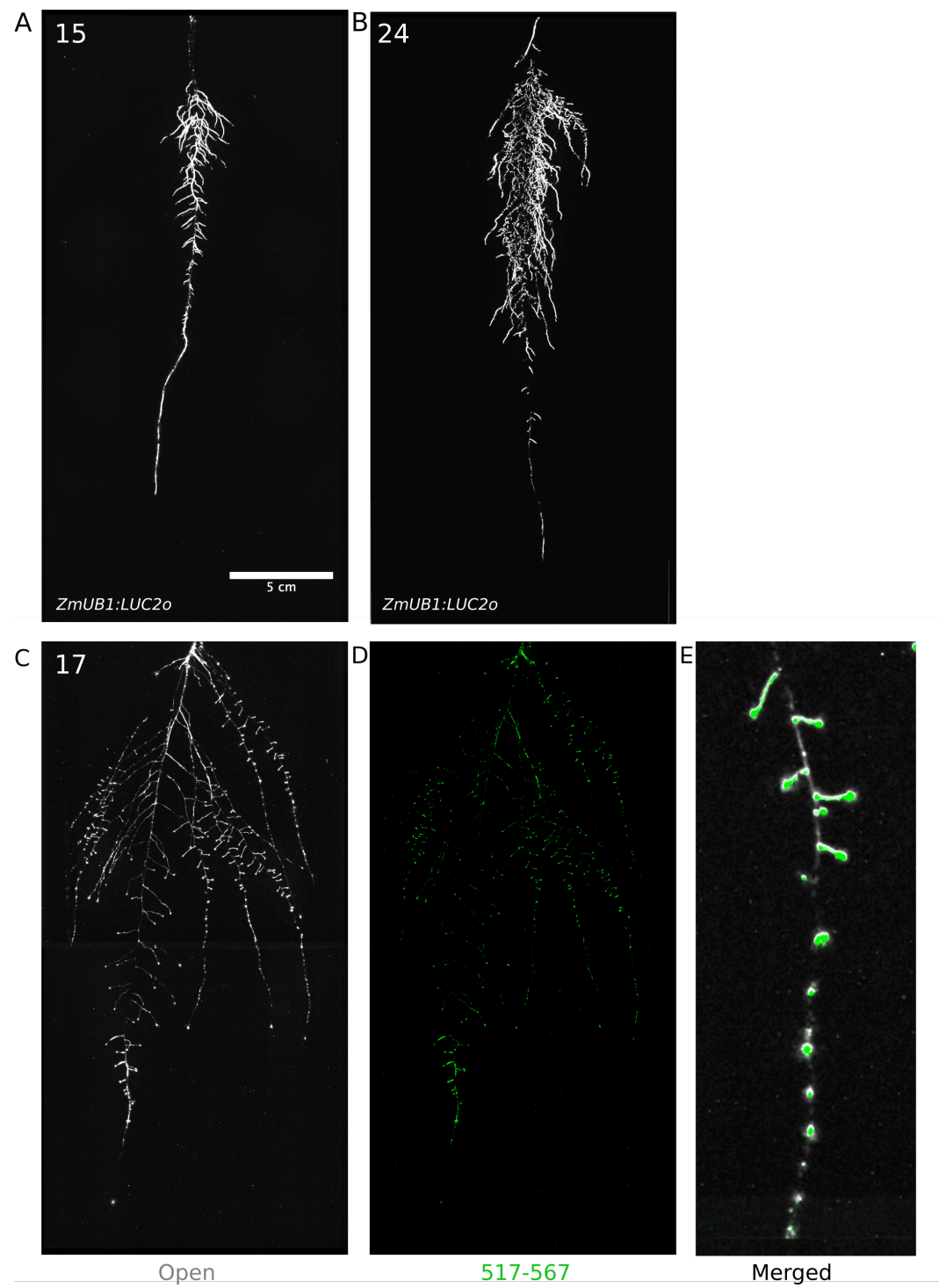


774 **Figure 6. Study of effect of water deficit on root system architecture.** A-D)
775 Root systems 22 DAS and exposed to water deficit 13 DAS onwards. Sample images of
776 well watered (left panels) and water deficit (right panels) root systems treated from 13
777 to 22 DAS and directionality (line graphs to left of images) for (A) Col-0 (B) Bay-0 (C) *miz1*
778 mutant and (D) *tir1-1*. E) Root system of a 22 DAS plant exposed to water deprivation
779 from 9 DAS onwards with magnified view of lateral root primordia (F). G) The same
780 root as in (E) 24 hours after rewatering and magnified view of lateral root primordia (H).
781 Kolmogorov-Smirnov test at $p < 0.001$ was used to compare directionality distributions
782 between the different treatments and genotypes. A Local Polynomial Regression Fitting
783 with 95% confidence interval (grey) was used to represent the directionality distribution
784 curve. 0° is the direction of the gravity vector.
785



786

787 **Figure 7. Relationship between local soil moisture content and root growth**
 788 **direction.** Data quantified from the time lapse series shown in [Video 2](#). Density plots
 789 shown at periphery of graph for root direction (x-axis) and soil moisture (y-axis). 0° is
 790 the direction of the gravity vector. Data represents 2535 root tips measured in a series
 791 encompassing 10 time points.



792 **Figure 8:** Roots of *Brachypodium distachyon* transformed with *ProZmUB1:LUC2o* and

⁷⁹⁴ imaged at 15 (A) and 24 (B) DAS grown in control conditions. C) Open channel of 17
⁷⁹⁵ DAS tomato plant transformed with *ProeDR5rev:LUC2o* and *Pro35S:PPyRE8o* D) Green
⁷⁹⁶ channel showing only *ProeDR5rev:LUC2o* E) Amplification of the open and green channel
⁷⁹⁷ showing increased expression of *ProeDR5rev:LUC2o* reporter in early-stage lateral roots.

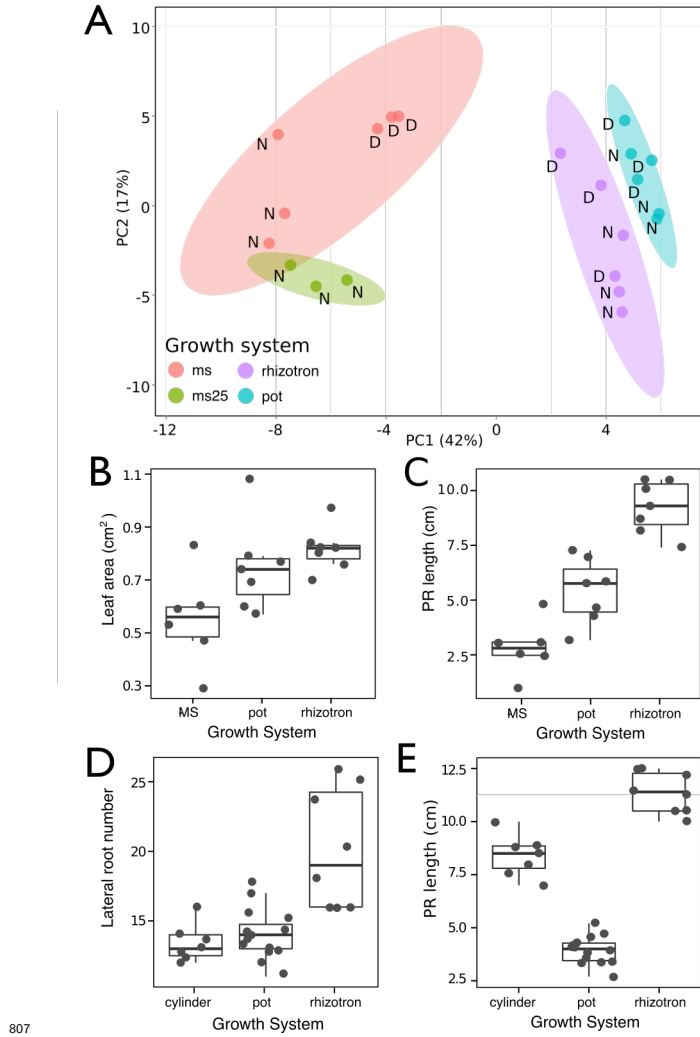
798 **Videos**

799 **Video 1** Time lapse from 11 to 21 DAS of a Col-0 plant expressing ProUBQ10:LUC2o
800 grown in control conditions

801 **Video 2** Time lapse from 16 to 24 DAS of Col-0 plants expressing *ProUBQ10:LUC2o*
802 growing in water deficient (left) and control (right) conditions. Plants were sown under
803 control conditions and water deficit treatment started 11 DAS. Images were taken every
804 day.

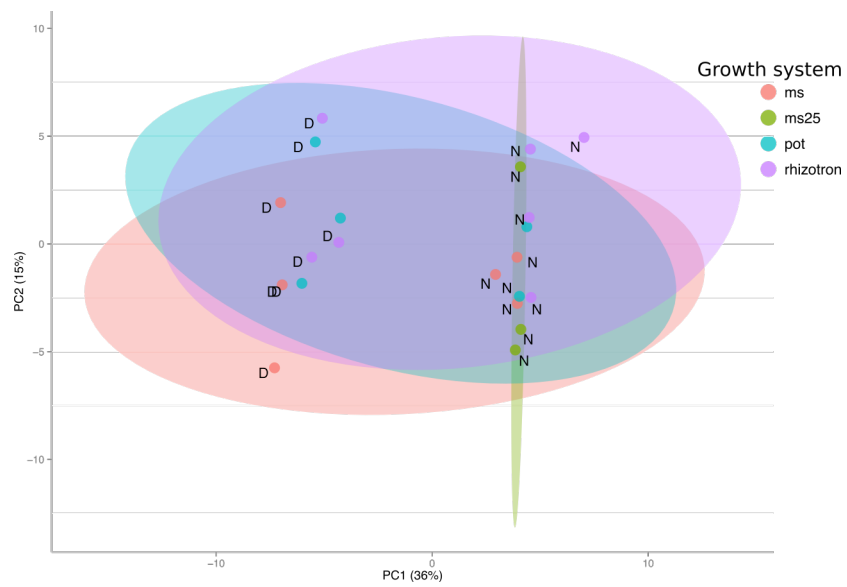
805 **Supplementary Material**

806 **Supplementary figures**



807
 808 **Figure 1-figure supplement 1. Effect of different growth systems on plant biol-**
 809 **ogy.** A) Principal Components Analysis (PCA) score plot of a set of 76 genes analyzed by
 810 qPCR from root samples of plants grown in MS plates, pots, and rhizotrons. After 15 DAS
 811 three plants were collected at the end of the day (D) and three were collected at the end of
 812 the night (N). (ms = plant grown in full ms and 1% sucrose, ms25 = plants grown in 25%
 813 of full ms) B) Lateral root number and G) primary root length of 18 DAS plants grown in

⁸¹⁴ 30 cm tall cylinders, pots and rhizotrons, all with a volume of 100 cm³ (n = 6-12 plants).
⁸¹⁵ D) Leaf area and E) primary root length of plants of the same age (15 DAS) as the ones
⁸¹⁶ used for the qPCR experiment (n= 6-7). ANOVA analysis with p < 0.01 was used to test
⁸¹⁷ significant differences between the different parameters.

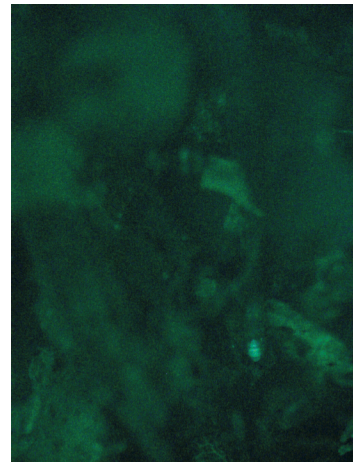


818 *Figure 1-figure supplement 2. PCA plot of shoots of the same samples analyzed in Figure
 819 1. See Figure 1 for more details regarding experimental conditions used.
 820



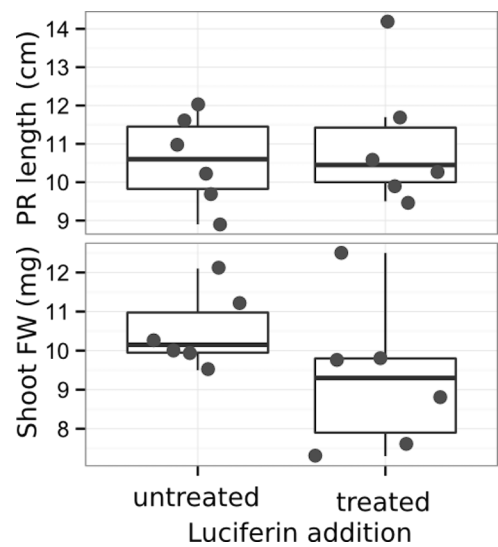
Brightfield

821



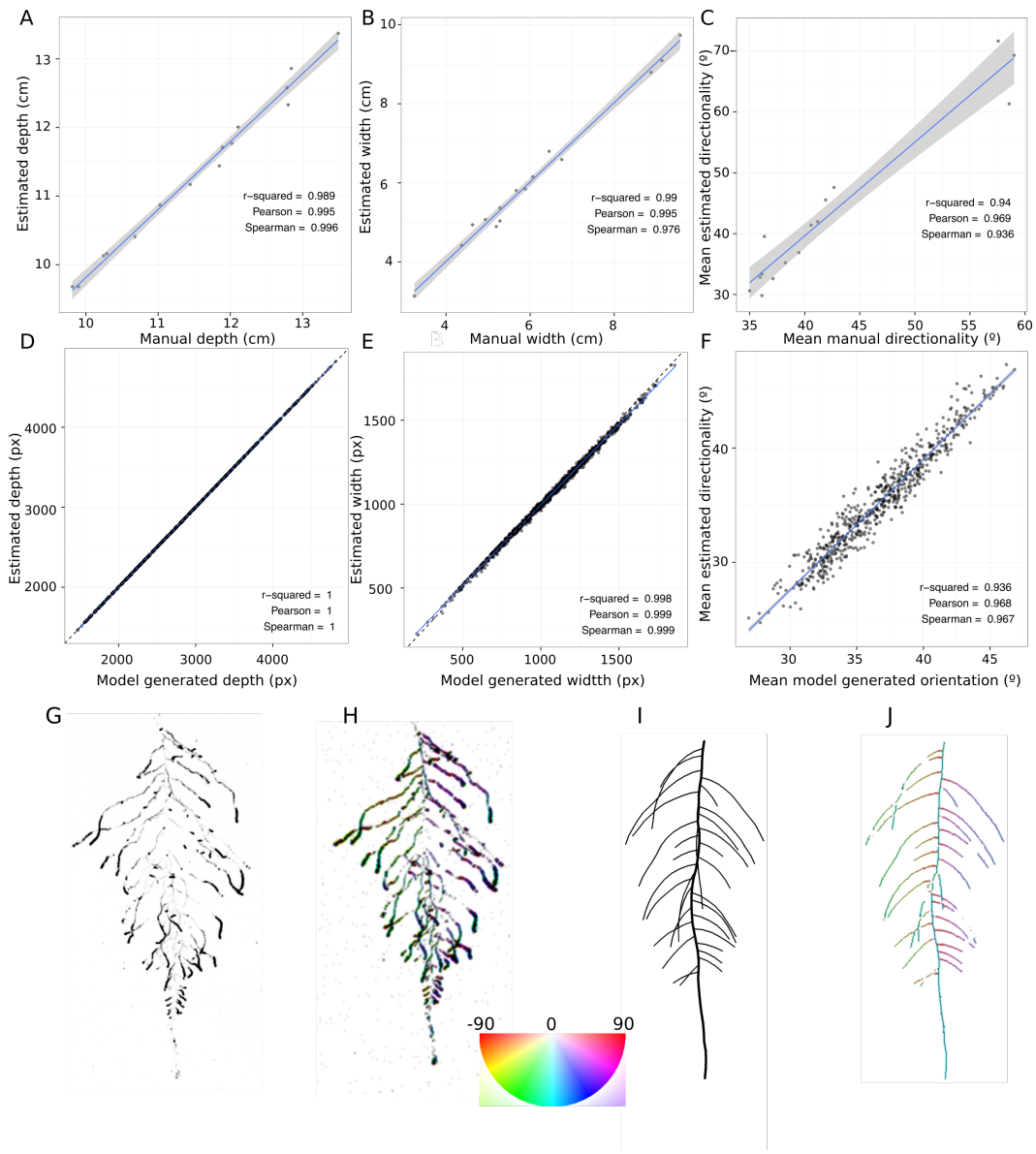
GFP

822 **Figure 1-figure supplement 3** Image of an Arabidopsis root in soil imaged with white
823 light (brightfield) or epifluorescence.



824

825 **Figure 1-figure supplement 4** Effect of luciferin addition on primary root length and
 826 shoot size of 14 DAS seedlings that were either continuously exposed to 300 μ M luciferin
 827 from 9 DAS after sowing or not.



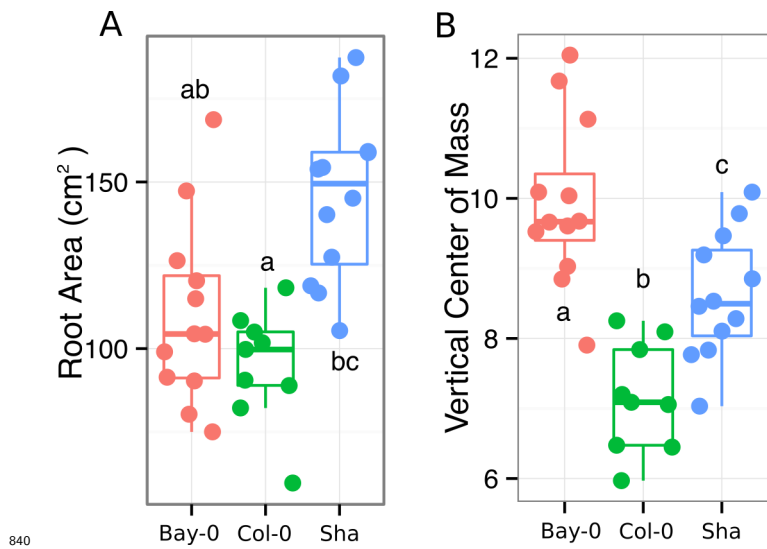
828

829 **Figure 1-figure supplement 5** GLO-RIA ground truth comparison. Tests of GLO-RIA
 830 were performed using two approaches. We first manually quantified root system depth (A)
 831 width (B) and average lateral root angle (C) in a set of 15 root systems corresponding
 832 to different *Arabidopsis* accessions. We also generated 1240 contrasting root systems
 833 using ArchiSimple and quantified root system depth (D) width (E) and directionality
 834 (F) using GLO-RIA. Example of a real (G) and ArchiSimple generated (H) root system

⁸³⁵ and corresponding GLO-RIA determined directionality color-coded into the image (I, J).

⁸³⁶ Absolute orientation angle values are taken before all calculations.

⁸³⁷ **Figure 1-figure supplement data 1:** Two way ANOVA P-values comparing plants grown
⁸³⁸ in MS media vs. plants grown in soil (pots or rhizotrons) and plants collected at day or night.
⁸³⁹ We used p-value < 0.00065 threshold based on Bonferoni adjustment for multiple testing.



840
841 **Figure 3-figure supplement 1** A) root area, B) vertical center of mass of Bay-0, Col-0
842 and Sha accessions.

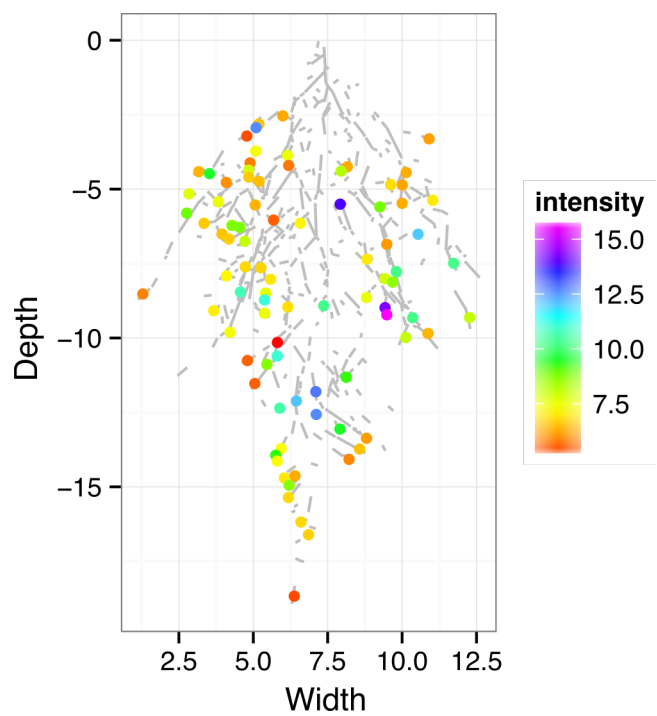
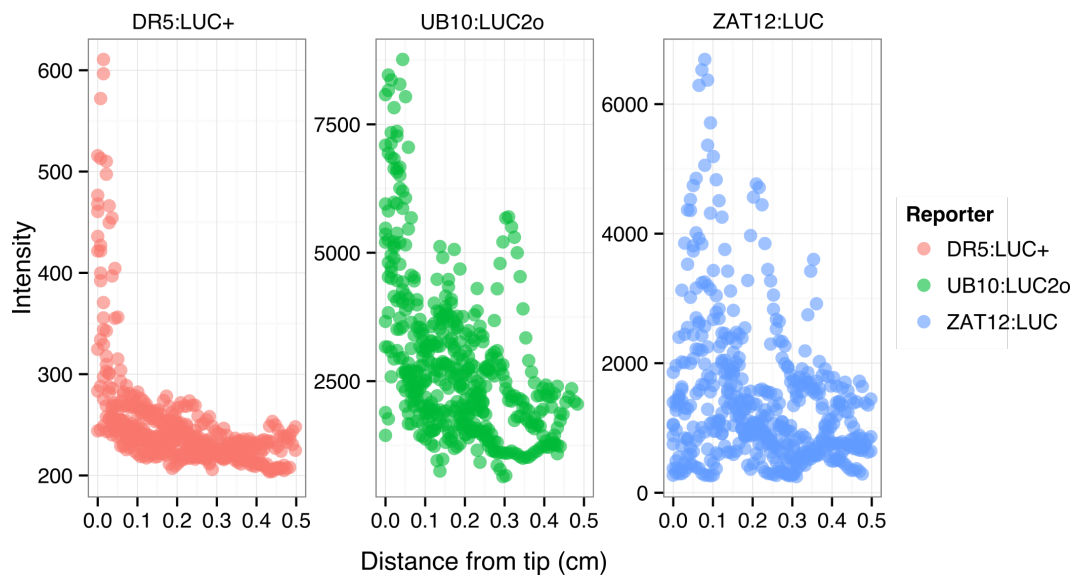


Figure 4-figure supplement 1:

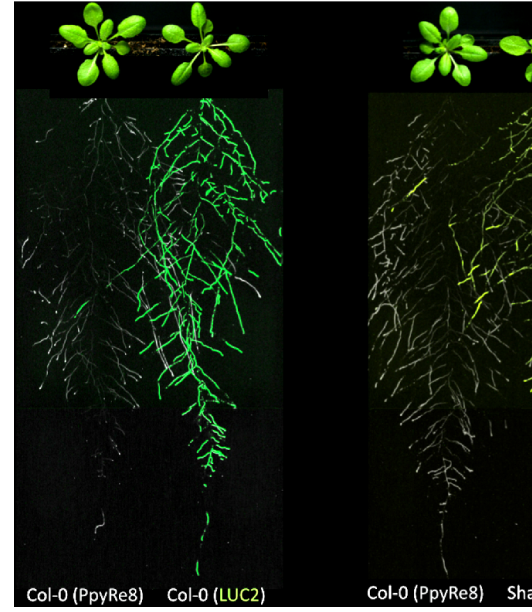
843

844 ZAT12:LUC intensity and root segments automatically identified with GLO-RIA.

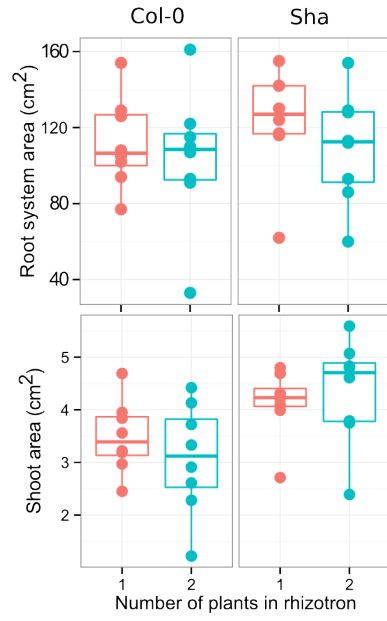


845 **Figure 4-figure supplement 2:** DR5:LUC+, UBQ10:LUC2o and ZAT12:LUC intensity
 846 values along the root tip. Data was manually obtained by obtaining the intensity profile
 847 of the first 0.5 cm from the root tip of individual lateral roots. Ten lateral roots for each
 848 reporter were measured.
 849

850

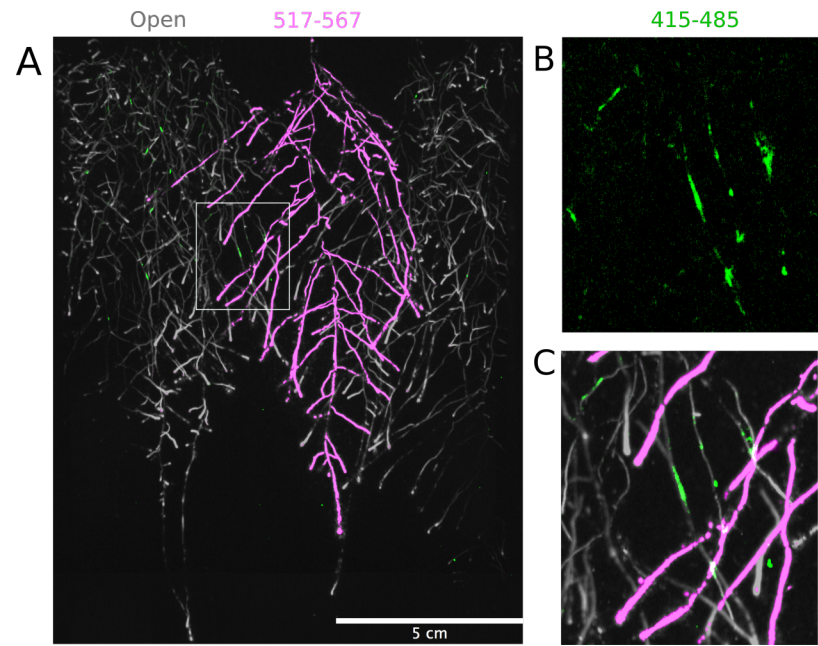


851



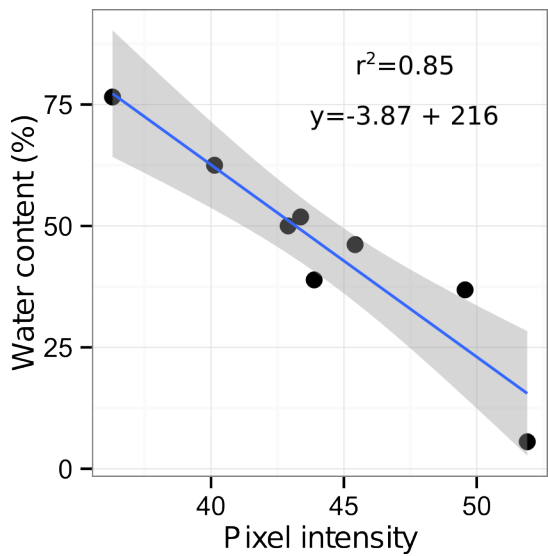
852 **Figure 4-figure supplement 3.** Images of plants at 22 DAS growing in the
 853 same rhizotron and expressing different luciferases. A) Two Col-0 plants expressing
 854 *ProUBQ10:LUC2o* and *ProACT2:PPyRE8o* B) Col-0 plant expressing *ProACT2:PPyRE8o*
 855 and Sha plant expressing *ProUBQ10:LUC2o*.

856



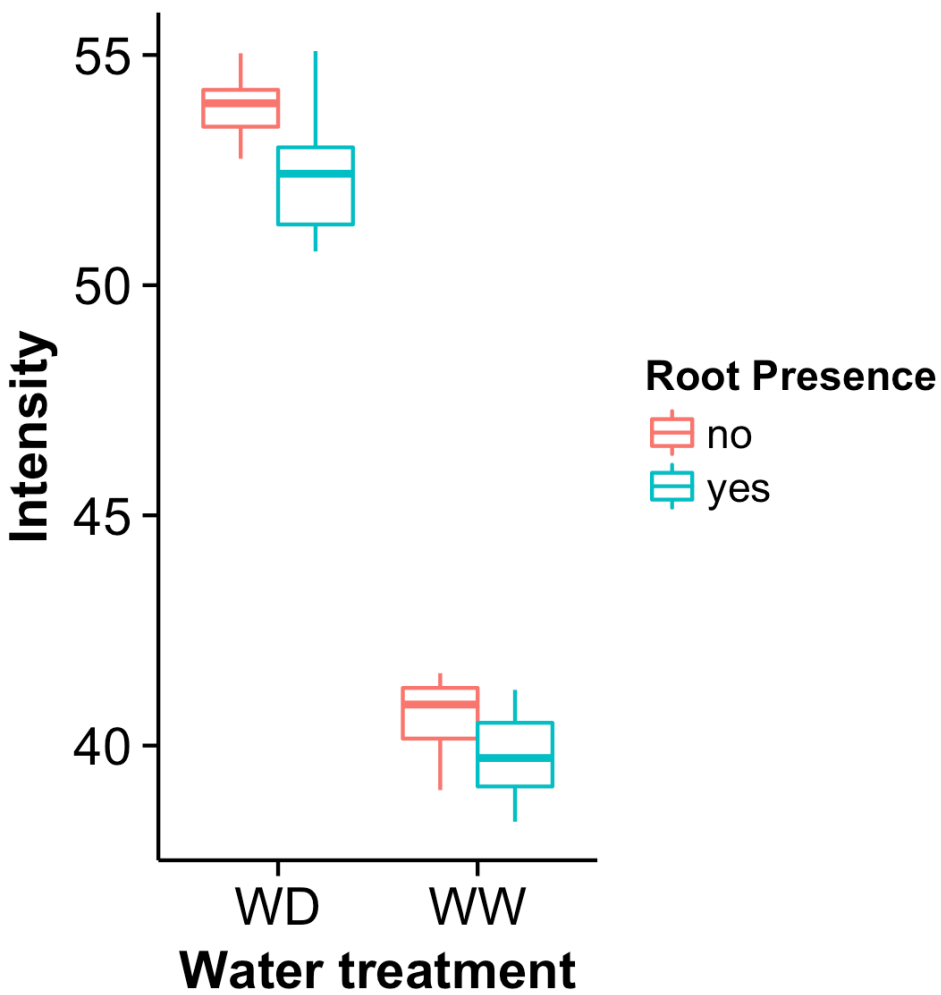
857 **Figure 4-figure supplement 4. Three-reporter-based analysis of root-root-**
 858 **microbe interactions.** A) Image showing a 22 DAS *ProUBQ10:LUC2o* plant (magenta)
 859 grown in the same rhizotron with *ProACT2:PpyRE8o* plants (grey). Plants were inoculated
 860 with *Pseudomonas fluorescens* CH267 (green). Magnified portion of root systems colonized
 861 by *Pseudomonas fluorescens* showing *P. fluorescences* (B) only or all three reporters
 862 together (C).

863



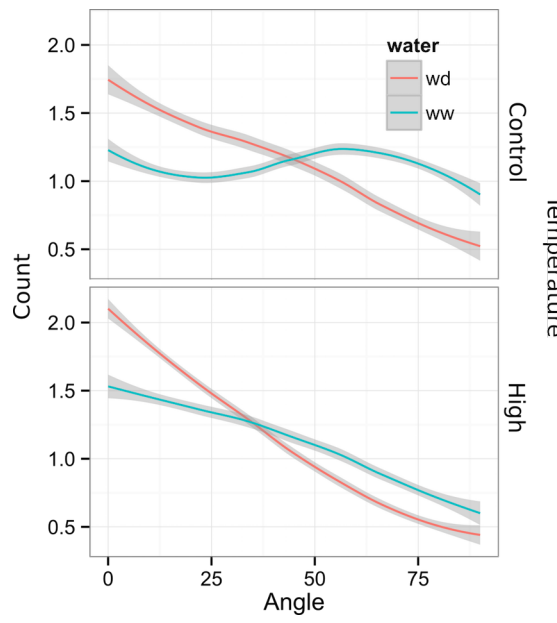
865 **Figure 5-figure supplement 1:** Moisture calibration curve. Rhizotrons with different
866 levels of moisture were prepared and scanned to obtain readings of pixel intensity. Soil from
867 rhizotrons was then weighed, dried down in an oven at 70 °C for 48 hours and percent water
868 content quantified.
869

870



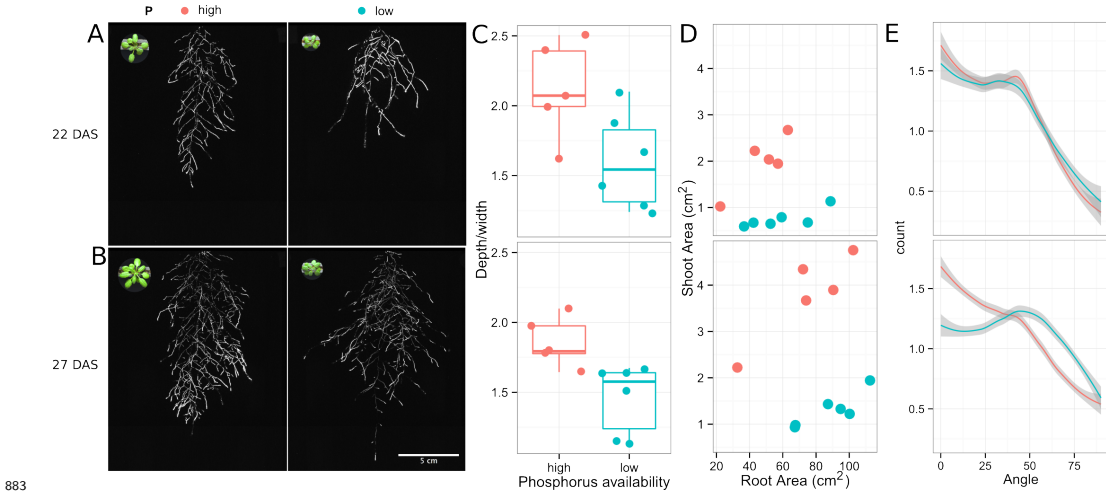
871
872 **Figure 5-figure supplement 2.** Comparison of soil intensity values between
873 **areas of the rhizotron with or without the presence of roots, determined based**
874 **on luminescence data.** Mean intensity values from 100 x 100 pixel squares samples of
875 both areas were obtained from 10 different rhizotrons. Wilcoxon test analysis with $p < 0.01$
876 was used to test significant differences between areas with our without root presence.

877



878 **Figure 6-figure supplement 1** Directionality analysis of roots of plants transferred to
 879 water deprivation conditions after 9 DAS and kept 22 °C (control temperature) and 29 °C
 880 (high temperature) until 22 DAS. (0° is the direction of the gravity vector).
 881

882

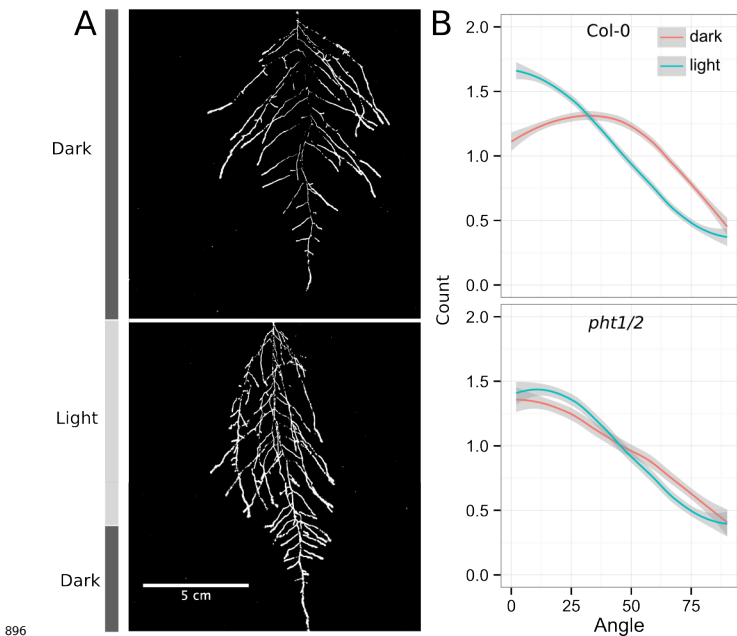


883 **Figure 6-figure supplement 2. Phosphorus deficiency response of root systems**

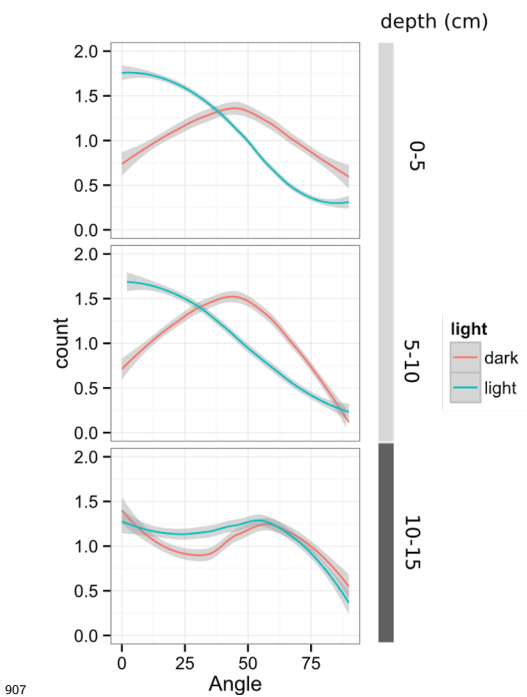
884 Shoot and root systems of *ProUBQ10:LUC2o* Col-0 plants growing in soil supplemented
 885 with 1ml of 100 μ M P-Alumina (left) and 0-P-Alumina (right) 22 (A) or 27 (B) DAS. C)
 886 Root depth/width ratio of 22 (top) and 27 (bottom) DAS plants. D) Scatter-plot showing
 887 relationship between root and shoot system area at 22 (top) and 27 (bottom) DAS. E)
 888 Root directionality distribution in plants 22 (top) and 27 (bottom) DAS. Anova analysis at
 889 p < 0.01 was used to compare depth/width ratios in P treatments. Kolmogorov-Smirnov
 890 test at p < 0.001 was used to compare directionality distributions between the different
 891 treatments. A Local Polynomial Regression Fitting with 95% confidence interval (grey)
 892 was used to represent the directionality distribution curve.(0° is the direction of the gravity
 893 vector).

894

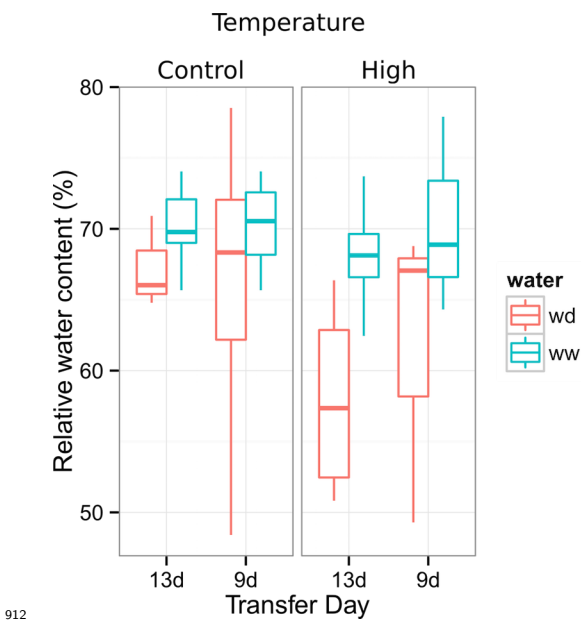
895



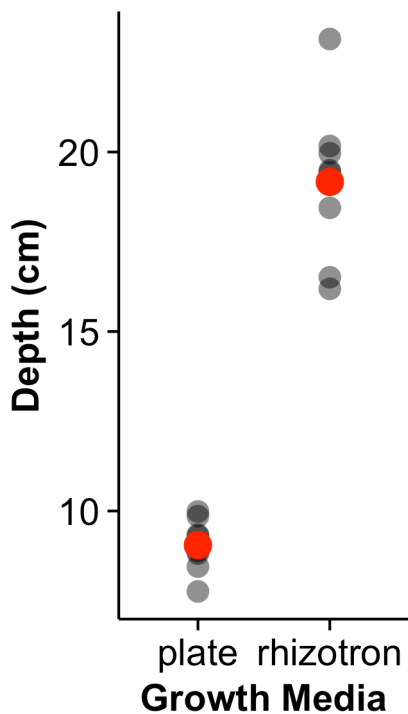
896
897 **Figure 6-figure supplement 3. Effect of light on root directionality.** A) Col-0
898 root systems shielded (top) or light exposed (bottom). After 9 DAS the top third of the
899 rhizotron was exposed to light (indicated on the side with a light grey bar) and plants were
900 imaged at 20 DAS. B) Directionality analysis of root systems shielded (red) or exposed
901 (green) to light for Col-0 (top panel) or *pht1/2* double mutant (bottom panel). Between
902 4 and 6 plants were analyzed per treatment. ANOVA analysis at $p < 0.01$ was used to
903 compare depth/width ratios in P treatments. Kolmogorov-Smirnov test at $p < 0.001$ was
904 used to compare directionality distributions between the different treatments. A Local
905 Polynomial Regression Fitting with 95% confidence interval (grey) was used to represent
906 the directionality distribution curve.(0° is the direction of the gravity vector).



907
908 **Figure 6-figure supplement 4** Plots showing output of directionality analysis performed
909 at different depths (0-5, 5-10, 10-15 cm) in rhizotrons exposed to light or kept in the dark.
910 (0° is the direction of the gravity vector).
911



912 **Figure 6-figure supplement 5.** Leaf relative water content of 23 DAS plants that
 913 were subjected to water deprivation (WD) after 9 or 13 DAS or kept under
 914 well watered (WD) conditions. At 9 DAS half of the plants were kept under control
 915 temperature conditions (22 °C) and the other half transferred to a 29 °C (high) chamber. n
 916 = 6-8 plants.
 917
 918



919

920 **Figure 8-figure supplement 1** Depth of the primary root of *Brachypodium* plants grown
921 in rhizotrons or on gel-based media (n=8-11). Red dots indicate mean values.

922

923 **Supplementary material**

924 **Supplemental Material 1**

925 Blueprints of the holders, clear sheets and spacers needed to built the rhizotrons. Additional
926 details are provided in the materials and methods. Files are provided in Adobe Illustrator
927 .ai and Autocad .dxf formats.

928 **Supplemental Material 2**

929 Primers used in the qPCR experiment.

930 **Supplemental Material 3**

931 Vector maps of all the constructs used in this work.

932 **Source data files**

933 Source data files used for building the following figures are provided: Figure 1-source data

934 1

935 Figure 1-figure supplement 1-source data 1

936 Figure 1-figure supplement 2-source data 1

937 Figure 1-figure supplement 3-source data 1

938 Figure 1-figure supplement 5-source data 1

939 Figure 2-source data 1

940 Figure 3-source data 1

941 Figure 3-source data 2

942 Figure 3-figure supplement 1-source data 1

943 Figure 4-source data

944 Figure 4-figure supplement 1-source data 1

945 Figure 4-figure supplement 2-source data 1

946 Figure 5-figure supplement 1-source data 1

947 figure_5_figure_supplement_1.csv

948 Figure 6-source data 1

⁹⁴⁹ Figure 6-figure supplement 2-source data 1

⁹⁵⁰ Figure 6-figure supplement 3-source data 1

⁹⁵¹ Figure 6-figure supplement 4-source data 1

⁹⁵² Figure 6-figure supplement 5-source data 1

⁹⁵³ Figure 7-source data 1

⁹⁵⁴ Figure 8-figure supplement 1-source data 1